Journal of Polymer Research (2019) 26: 220
https://doi.org/10.1007/s10965-019-1896-0

ORIGINAL PAPER

Structure and properties of epoxy polymer nanocomposites reinforced with carbon nanotubes

Vadim I. Irzhak[1] · Gulzhian I. Dzhardimalieva[1] · Igor E. Uflyand[2]

Received: 16 April 2019 / Accepted: 17 August 2019 / Published online: 20 August 2019

Abstract

A detailed analysis of nanocomposites based on epoxy polymers and various nanofillers, including one-, two- and three-dimensional carbon nanotubes, was carried out. Special attention is paid to the structure of epoxy nanocomposites and the interfacial layer in these systems. The data on the mechanical, electrophysical, magnetic, thermal, and tribological properties of epoxy nanocomposites are summarized. The influence of the nature of nanofillers (carbon nanotubes, metals, and minerals) on the properties of nanocomposites is analyzed. The problems and prospects of development of nanocomposites based on epoxy polymers reinforced with carbon nanotubes are considered.

Keywords Carbon nanotubes · Epoxy polymers · Graphene · Nanocomposites · Nanofillers

Introduction

From the point of view of a set of properties, epoxy polymers stand out among other polymeric materials and play an important role in the aerospace, automotive, shipbuilding and other industries. Their widespread use in technology is associated, firstly, with the high processability of epoxy resins and, secondly, with the unique combination of the performance characteristics of their curing products [1–4].

The high reactivity of epoxy groups and the thermodynamic miscibility of epoxy oligomers with many substances allow the use of different curing agents and carry out curing reactions under various technological conditions [5–7]. Of no less importance are the features of the synthesis processes, such as the absence of volatile products and low shrinkage.

Epoxy polymers have high values of static and impact strength, hardness and wear resistance. They have a pronounced thermal stability and heat resistance. Many solid surfaces form strong adhesion bonds with epoxy polymers [1, 2, 8–10]. This circumstance determines their use as compounds, glues, paint materials and coatings, including in aerospace engineering.

Composite materials, including fibrous materials [11], primarily high-filled reinforced plastics, in which high-modulus and high-strength fibers function as load-bearing elements, occupy a special place [12]. The matrix is mainly designed to realize the properties of composites in an engineering material. It ensures the integrity of the material, as well as the transfer and distribution of internal stresses. Epoxy polymers fully meet these criteria.

Apparently, epoxy nanocomposites are designed to implement the same degree of unique functional properties of nanoparticles (NPs): electrical, magnetic, optical, chemical, and biological.

Complicated information about epoxy nanocomposites is contained in [13–16]. Reviews [17–21] are devoted to epoxy nanocomposites with carbon nanotubes (CNTs). CNTs are of particular interest because of their low density, high compression ratio, high strength, high ductility, light weight, and exceptional mechanical, thermal, optical, and electrical properties. These unique characteristics make it possible to consider CNTs as ideal fillers for the manufacture of light-weight polymer composite materials with improved mechanical performance and multifunctional properties. Therefore, the incorporation of CNTs in epoxy polymers leads to an increase in the resulting material's strength and the fracture toughness. It is important that the level of reinforcement depends on many

✉ Igor E. Uflyand
ieuflyand@sfedu.ru

[1] Institute of Problems of Chemical Physics RAS, Chernogolovka, Moscow, Region, Russian Federation

[2] Department of Chemistry, Southern Federal University, Rostov-on-Don, Russian Federation

factors, in particular, on the nature of the CNT, surface modification, orientation of the CNT, the amount of CNTs and the polymer/nanotube interfacial bonding [22–28]. Some aspects of epoxy nanocomposites containing graphene were covered in [29–32].

In this review, we took the opportunity to conduct a comparative analysis of epoxy nanocomposites containing nanoparticles of metals and minerals, graphene and CNTs, as well as to discuss their structure and properties. Taking into consideration the urgency of the problem, the growing volume of publications in this area and the availability of recent research not covered in the mentioned reviews, we consider the appearance of such an article to be very timely.

Structure of epoxy nanocomposites

The properties of polymer nanocomposites are determined by the structure of the matrix, the type and character of the distribution of NPs within the bulk, and finally, the size and nature of the interfacial layer. In the case of epoxy nanocomposites, these factors are largely incorporated in the synthesis stage. Many examples are given above both for the matrix and for the distribution of, say, *montmorillonite* (MMT) within the volume. However, the question of the formation of the interfacial layer remained open.

As has been shown in many papers, mostly using the nanoindentation method [33, 34], regardless of the nature of the fiber and the matrix, the interfacial layer extends to micrometers in polymeric fibrous composites. Obviously, the same situation should be expected in the case of nanocomposites.

Indeed, the surface energy of NPs is quite large; therefore, they are characterized by the adsorption of various molecules. Components of epoxy binders are no exception [35–37]. It should be kept in mind that the structures of the adsorption layers are different for one-dimensional (1D) CNTs, two-dimensional (2D) graphene, three-dimensional (3D) fullerene, and metal-containing NPs [38]. In the latter case, agglomeration of particles is possible, accompanied by the development of fractal structures with peculiar adsorption properties [39].

CNTs and graphene can be non-covalently functionalized without distorting the morphological structure by formation of π-π-bonds with aromatic compounds, corresponding polymers and surfactants through ionic interactions [35, 36, 40, 41]. The silicate surface of MMT and halloysite NPs [42] is modified by organic compounds, including amines and silanes [43, 44]; in this case, ionic bonds can be form.

Alkylamine-type compounds react with NPs of metals and their oxides to form Mt-N bonds [45, 46]. The same behavior is typical of alkylthiols. But if S-Mt bonds exist, then the potential of attraction between the alkyl chain and the surface of NPs is such that the adsorbed molecules form bonds with the maximum possible number of surface metal atoms [47].

At the same time, molecular dynamic calculations of the surface area (σ_r) of alkanethiols adsorbed by spherical gold NP [48] showed that σ_r decreases with decreasing radius (r) according to the following formula (1):

$$\frac{\sigma_r}{\sigma_f} = \left(1 + \frac{0.8}{r}\right)^{-1} \quad (1)$$

where σ_f is the footprint of the alkanethiol molecule on a flat surface, and r is in nm.

It was shown that, starting with hexanethiol, the value of σ_r does not depend on the ligand length. Calculations are consistent with experimental data [49].

Thus, adsorption causes the formation of an interfacial layer.

Another factor contributing to the stable interfacial interaction of NPs with the matrix is their covalent functionalization [50–52]. It should be noted that, unlike the non-covalent modification, the covalent modification can introduce defects into the structure of NPs. For example, the introduction of surface COOH-groups by oxidation of CNTs leads to tube bending and, thus, deteriorates its mechanical and conductive properties [53]. Note that the presence of reactive groups on the surface of NPs allows them to be used for the introduction of the corresponding ligands by grafting-from [54] or grafting-to [55].

Finally, one should take into account the peculiarity of epoxy nanocomposites, namely, that the synthesis of an epoxy matrix occurs, as a rule, at elevated temperatures, and the resulting material is used at room temperature. Due to the difference in the thermal expansion coefficients of the filler and the matrix, the interfacial layer can be deformed to a certain extent.

The glass-transition temperature (T_g) characterizes the matrix, since it is a function of its molecular architecture and depends on parameters such as the functionality of the epoxy oligomer and curing agent, as well as the degree of conversion. The study of the processes of curing the matrix in the presence of NPs shows (see above) that an unambiguous conclusion about their effect on T_g is hardly possible.

A. Allaoui and N.-E. El Bounia [56] analyzed the published data and suggested that if single-walled CNTs (SWCNTs) can lead to a decrease in T_g due to their tendency to aggregate, then multiwall CNTs (MWCNTs) tend to increase or not to change the T_g of epoxy nanocomposites. However, K.W. Putz et al. [57] demonstrated that the influence of MWCNTs (0.25 and 0.5 wt.%) on T_g depends on the density of the matrix network: T_g grows in loosely cross-linked networks, and T_g decreases in densely cross-linked networks. It is assumed that in these cases the interfacial interaction is crucial. In loose networks, the filler limits the mobility of the kinetic fragments due to their adsorption, whereas in dense MWCNTs it prevents the formation of network junctions.

The formation of interfacial layers, both in the absence of covalent functionalization and in its presence, was proved in [58]. SWCNTs and MWCNTs were treated with a mixture of nitric and sulfuric acids; as a result, carboxyl groups appeared on the surface. The latter were converted to ester groups by reaction with phenylglycidyl ether. The matrix was obtained by curing diglycidyl ether of bisphenol A (BADGE) with poly(ether triamine). The difference in the treatment procedure is reflected in the structure of the interfacial layer, which is manifested in relaxation spectra. As evidenced by the pattern of the tan δ(*T*) curves obtained at a frequency of 0.1 Hz (Fig. 1), a high-temperature transition typical of the matrix (curves *1*) is recorded for composites, based on both SWCNTs and MWCNTs. But in the case of unmodified (curves *2*) and COOH-modified (curves *3*) CNTs, an additional transition is observed at a lower temperature. This conclusion indicates the presence of a structure that is less perfect than the structure of the matrix and, apparently, is localized in the interfacial layer. The authors believe that the observed effect is associated with selective adsorption of epoxy oligomer on tubes, which is hardly possible when ester fragments appear on the surface (curves *4*). Another explanation for this effect is also possible: ester tails facilitate the relaxation of stress of the interfacial layer. Note that in the case of SWCNTs, the effect is more pronounced than the effect for MWCNTs. This is an obvious consequence of the fact that CNTs are modified to a greater degree (8.6% versus 4.9% with respect to carboxyl groups and 21.1% versus 13.7% with respect to ester fragments).

S. Wang et al. [59] estimated the shear strength of the SWCNT/epoxy matrix interface as 306 MPa under the assumption that tubes are not clustered and that the grafting of diethyltoluenediamine leads, on average, to the formation of one bond per 25 carbon atoms. In accordance with the same calculations, the strength of the interfacial layer in the case of unmodified SWCNTs is ~50 MPa. However, it should be borne in mind that the strength of the interfacial layer (τ) depends on the radius of CNTs. For example, according to the data [60], obtained by pulling out of a polyethylenebutylene matrix, $\tau \approx 85$ MPa for MWCNTs with a radius of 10–20 nm and it drops to ~15 MPa at 60–70 nm.

A number of methods for covalent modification of CNTs and manifestation of their functionalization in the properties of epoxy nanocomposites is discussed in reviews [19, 50]. The methods used for the functionalization of graphene, which in principle do not differ from those used in the previous cases, are described in [40, 61–63]. For example, a graphene dispersion in a mixture of methylsulfonic acid and P_2O_5 was acylated by dicarboxylic acid (4,4′-dicarboxy-diphenyl ether), and then the polycondensation reaction with 3,3′-diaminobenzidine was carried out in situ to obtain the grafted polybenzimidazole [61]. As in the case of CNTs, an important circumstance is the disaggregation of graphene sheets [64], taking into consideration that the latter shows a tendency to aggregation in an epoxy matrix.

Graphene oxide (GO) is often used as an initial reagent in covalent functionalization, which is obtained, in particular, by the oxidation of graphite. For example, amino and epoxy-functionalized GO were synthesized using silane binders: 3-aminopropyltriethoxysilane and 3-glycidoxypropyltrimethoxysilane [65].

Alkylamines consisting of long-chain hydrophobic alkyl groups and hydrophilic amino groups are grafted onto the surface of GO due to the presence of two types of reactive groups on it, namely carboxyl and epoxy. The first groups participate in the amidation reaction, while the latter groups

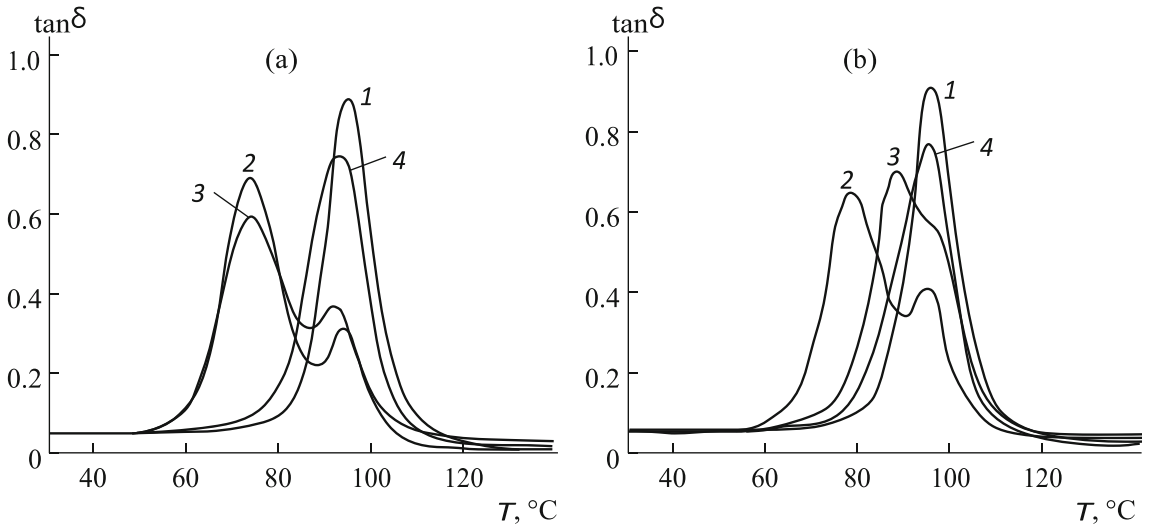

Fig. 1 Temperature dependence of tanδ of epoxy matrices and epoxy nanocomposites containing 1 wt.% of (**a**) SWCNTs and (**b**) MWCNTs. The neat resin (*1*) and the epoxy nanocomposite with unmodified NPs (*2*) and NPs modified with COOH groups (*3*) and grafted ester fragments (*4*). The data are taken from [58]

participate in the nucleophilic substitution reaction [66]. The use of bifunctional poly(ester diamine) makes it possible to graft amino-containing fragments capable of reacting with epoxy groups of the binder [67]. Molecules with different chain lengths (D230 and D2000) were used. It was assumed that various interface structures between the filler and the matrix will be created. The grafting of D230 chains onto the GO surface leads to the limited segment mobility and, accordingly, to minimal deformability. D2000 chains have much greater deformability due to their greater length. This helps to increase the mobility of the filler in the matrix and causes scattering of energy during deformation. As a result, the interphase obtained using D230 and D2000 leads to a difference in the mechanical properties of nanocomposites.

R. Konnola et al. [68] using the ratio (2) estimated the volume fraction of the interphase (v_{int}) in epoxy nanocomposites, in which the pristine GO and GO with the grafted copolymer of acrylonitrile and butadiene were used as fillers.

$$tg\delta = \frac{tg\delta_m}{1 + 1.5B\phi} \quad (2)$$

Here tgδ and $tg\delta_m$ are the values of the loss tangent of the nanocomposite and the matrix with the volume fraction of the filler ϕ, and B is the parameter that essentially characterizes the volume of the interfacial layer: $B = 1 + (\Delta R/R_0)^3$, where R_0 is the radius of NP, and ΔR is the thickness of the interfacial layer. Calculations showed that, for a filler concentration of 0.6 wt.%, the corresponding values of $B = 3.12$ and 8.84, v_{int} are 0.0040 and 0.0114.

Intercalation of various compounds in MMT is possible [69, 70], which, after exfoliation of the filler, is actually an interfacial layer. With this aim in view, L. Yang et al. [71] used 2-(3,4-dihydroxyphenyl)ethylamine, which was involved in the oxidative polymerization, and the surface of the MMT was covered by the obtained polymer. The interlayer distance increased during the polymerization.

In [72], epoxy nanocomposites based on bentonite modified with diphenylamine-4-diazonium via ion exchange were obtained. The interfacial layer was formed by the oxidative polymerization of aniline. The aryl groups of the diazonium strongly influence the interfacial interaction as a means of effective stress transfer.

In recent years, composites with halloysite nanotubes have attracted increasing attention of researchers [43, 52, 73, 74]. Halloysite is a kaolin rolled up to multi-walled tubes with an external diameter of nearly 50 nm, an internal diameter of ~15 nm and a length of 700 to 2000 nm. Composites based on them can store and dose chemical reagents and biologically active compounds (bactericides, antibiotics and other drugs) for a long time. Additives to various polymeric materials give them the desired mechanical properties while preserving their low density [75]. Obviously, the interfacial interaction plays not the last role here.

The peculiarity of the chemical structure of halloysite nanotubes is that their internal surface is covered by Al-OH groups, while the external surface mainly consists of siloxane groups Si-O-Si. Hence, it follows the strategy for modifying halloysite nanotubes aimed at creating an optimal interfacial layer: grafting of silanes is a common and common procedure for covalent functionalization [52].

Indeed, P. Sun et al. [76] successfully grafted 3-aminopropyltriethoxysilane onto the surface of halloysite nanotubes, pretreated with a mixture of H_2SO_4 and H_2O_2 in order to increase the concentration of hydroxyl groups having a higher activity towards silanization.

As regards metallic NPs, as noted above, adsorption often leads to the formation of chemical bonds [47]. For example,

$$RSH + Au_n(0) \rightarrow RS^-Au^+ - Au_{n-1}(0) + 1/2H_2;$$

that is, essentially, chemisorption occurs. Adsorbed molecules can form layers, the structure of which depends [75] on the concentration and nature of sorbates (for example, alkanethiols with the number of CH_2-groups below nine incapable of self-assembly [76]), temperature and sorbent. For example, molecular mechanics studies of A.P. Kaushik and P. Clancy [77] demonstrated that small (3 nm) and larger (6 nm or above) particles behave differently due to the different conformations of ligands on their surface. The length of the ligand is comparable to the lateral sizes of the facets of small metal-containing NPs. These molecules attempt to maximize interaction with the facets and, therefore, prefer to be horizontal in relation to the facet. As a result, ligands on small metal-containing NPs are usually localized by twisting around the core. Ligands on large particles with a larger number of ligands on the surface are in contact with each other and reduce the possibility of interaction with a metal core. Due to the large number of ligands on the surface, their horizontal position on the core facets is hardly possible due to steric hindrances and, therefore, they must be oriented vertically. Naturally, the interfacial interaction of the matrix with metal-containing NPs will also depend on their size.

The dependence of the ligand conformation on the size of metal NPs (Fig. 2) obtained in [76] makes it possible to calculate the distances from the surface of Au NPs to the functional (S) and "tail" (CH_3) groups of alkylthiol molecule.

It is seen that the first value does not depend on the particle size and decreases slightly with temperature. The second, reflecting the conformation of ligands, increases with increasing temperature and the stronger, the smaller the diameter of Au NPs.

Note that, on the one hand, the ligand layer protects NPs and thereby stabilizes it, but on the other hand, it makes it metastable, which leads to a decrease in the melting point, the main factor of which is the interchain interaction energy of ligands [47].

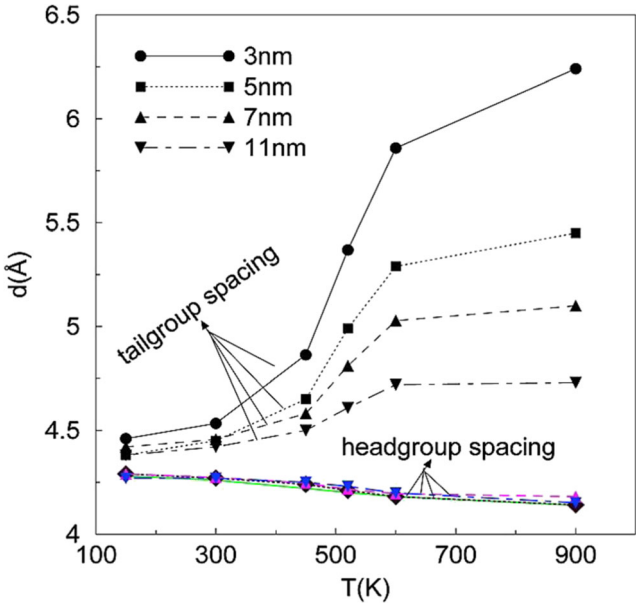

Fig. 2 Dependences of the conformation of the $CH_3(CH_2)_{13}SH$ ligand on the temperature and size of Au particles. The data are taken from [76]

Mechanical properties

The use of NPs as reinforcing agents for epoxy polymers involves solving problems common to polymeric composite materials, namely dispersing agglomerates and ensuring stress transfer from the matrix to the filler by creating the corresponding interfacial interaction. This requires consideration of the chemistry of the curing processes of the epoxy binder and the chemical and physical structures of the formed matrix.

In addition, it is necessary to take into account the size of NPs: one-dimensional, two-dimensional and three-dimensional fillers.

One-dimensional fillers: Carbon and halloysite nanotubes

CNTs and halloysite nanotubes can be considered as fibers of finite length. Mechanical properties, and not only they, depend on both the degree of filling and the aspect ratio χ (the length-to-diameter ratio). For example, in the case of unidirectional fibers with a small filling volume, the Young's modulus of the composite in the direction of orientation E_{11} is expressed through the eq. (3) [78]:

$$\frac{E_{11}}{E_m} = \phi_f A \tag{3}$$

where E_m is the modulus of the matrix, ϕ_f is the volume fraction of the fiber. Parameter A is a function of the modulus E_f and the fiber aspect ratio χ, as shown in Fig. 3.

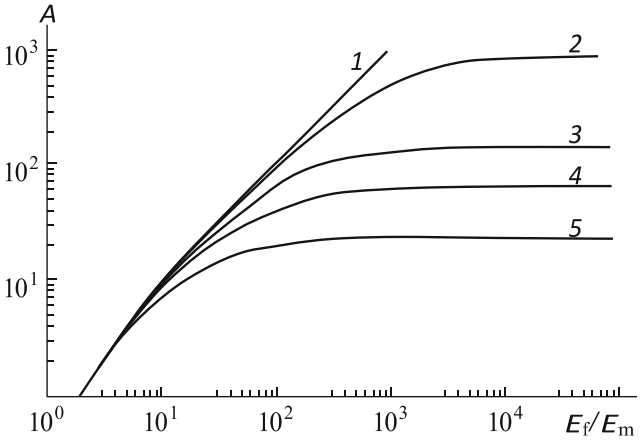

Fig. 3 Dependence of the Young's modulus of the unidirectional composite (parameter A) on fiber characteristics. $\chi^{-1} = 0$ (*1*), 0.01 (*2*), 0.03 (*3*), 0.05 (*4*), and 0.10 (*5*). The data are taken from [78]

At high values of fiber modulus (plateau region on the curves), the value of the parameter A is determined first of all only by the aspect. In the case of random orientation of the fibers, the modulus of the composite E_c can be represented as follows (4):

$$E_c = \frac{3}{8}E_{11} + \frac{5}{8}E_{22} \tag{4}$$

The transverse modulus E_{22} at a low filling can be calculated by the mix formula (5):

$$E_{22} = \frac{E_{tr}E_m}{E_{tr}\phi + E_m(1-\phi)} \tag{5}$$

Here E_{tr} is the transverse modulus of the fiber, and E_m is the modulus of the matrix with $E_{tr} \ll E_m$.

From formulas (3)–(5) it follows (6):

$$\frac{E_c}{E_m} = \frac{1}{8}\left(5 + \phi_f\left(3A + 5\frac{E_{tr}}{E_m} - 5\right)\right) \approx \frac{5}{8}(1-\phi_f) + \frac{3}{8}\phi_f A \tag{6}$$

that is, the parameter A gives the main contribution to the modulus value.

As can be seen from the Eq. (6) and Fig. 3, at a low filling ($\phi_f < 0.01$), the efficiency of the fiber becomes apparent only when $\chi \gg 10$.

In the ideal case (Kelly model), the strength of the composite (σ_c) obeys the mix rule (7) [78]:

$$\sigma_c = \eta\xi\left(1 - \frac{\sigma_f}{2\chi\tau}\right)\sigma_f\phi_f + \sigma_m(1-\phi_f) \tag{7}$$

where σ_f and σ_m are the fiber and matrix strength, η is the orientation factor equal to 0.2 for random distribution of fibers

over directions [79], ξ is the coefficient taking into account the level of realization of fiber properties, and τ is the shear strength of the interfacial layer.

Formulas (6) and (7) describe the ideal situation. In most studies, experimental data are matched to the Tsai-Halpin eq. (8) [80]:

$$\frac{E_c}{E_m} = \frac{1}{8}\left(3\frac{1+2\chi\eta_l\phi_f}{1-\eta_l\phi_f} + 5\frac{1+2\eta_t\phi_f}{1-\eta_t\phi_f}\right), \quad (8)$$

where.

$$\eta_l = \frac{E_f - E_m}{E_f + 2\chi E_m}, \quad \eta_t = \frac{E_f - E_m}{E_f + 2E_m} \quad (9)$$

M. Ayatollahi et al. [80] used formula (8) to interpret the obtained dependence of the modulus of epoxy nanocomposite on the concentration (0.1, 0.5 and 1 wt.%) and the aspect ratio (from 455 to 1000) of MWCNTs; the value of χ was changed by changing the diameter, not the length. These authors showed that satisfactory agreement between experimental data and calculations can be achieved by establishing $\chi \to a\chi^b$, $a = 0.0488$ and $b = 1.141$. It is assumed that this allows the imperfection of interfacial interaction, agglomeration and other possible drawbacks of the model (8).

As the aspect increased, the strength and fracture toughness of the epoxy nanocomposite increased. However, as was shown above, the growth of χ is associated with a decrease in diameter. Particles of smaller diameter create a stronger interfacial interaction with the matrix (see, for example, [60]). This facilitates the transfer of load and, accordingly, improves the mechanical properties.

A number of models that take taking into account the effect of the curvature of CNTs on the properties of the material were considered in [81–83]. For example, the authors of [81] put forward a new expression (10) for the rule of mixtures:

$$\frac{E_c}{E_m} = \frac{(k_1 k E_f - E_m)\phi_f}{E_f - (E_f - E_m)\phi_f}, \quad (10)$$

where.

$$k_1 = 1 - \frac{\tanh(2\chi\tau)}{2\chi\tau}, \quad \tau = \sqrt{\frac{-2E_m}{E_f(1-\mu)\ln\phi_m}} \quad (11)$$

Here μ is the Poisson's coefficient of the matrix; k is an empirical constant takes into account the orientation and curvature of CNTs. The authors were able to choose the values of $k < 1$, which describe the experimental data on the modules of epoxy nanocomposite by Eq. (10). The same considerations are used to interpret experimental strength data.

But researchers mostly use a modified Eq. (12)

$$\frac{E_c}{E_m} = \frac{1+2\chi\eta\phi_f}{1-\eta\phi_f}, \quad (12)$$

where.

$$\eta = \frac{E_f - E_m}{E_f + 2\chi E_m} \quad (13)$$

It is believed [83] that, due to the replacement $\chi \to \chi\exp\{-a-b\phi_f\}$, one can take into account the curvature of MWCNTs (Fig. 4).

The influence of various dispersion states of CNTs on the mechanical properties of epoxy nanocomposites is important. In particular, nanocomposites containing poorly dispersed CNTs exhibit a higher storage modulus, loss modulus, and complex viscosity than those of well dispersed CNTs [22].

Functionalization of CNTs has the greatest effect on the mechanical properties of the nanocomposite. For example, the modulus of epoxy nanocomposites containing 3% untreated MWCNTs or MWCNTs functionalized by treating with a mixture of aminobenzoic and polyphosphoric acids increased by 32 and 53%, respectively [84]. Note that the glass-transition temperature also slightly increased: 189 (matrix), 190 and 199 °C.

X. Chen et al. [85] showed that the ultimate tensile strength of the epoxy nanocomposite (1.5 wt.% filler) increases from 39 MPa (matrix) to 46 in the case of untreated MWCNTs and up to 59 MPa for MWCNTs functionalized by amino groups. T_g also increases from 98 to 109 and 112 °C.

The behavior of epoxy nanocomposites depends not only on the type of functional groups, but also on the structure of

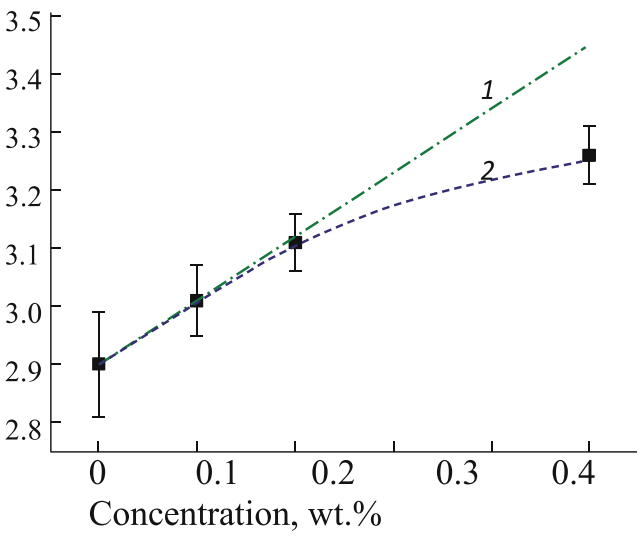

Fig. 4 Dependence of the elastic modulus of the epoxy nanocomposite on the concentration of MWCNTs (closed squares). (*1*) Eq. (12) and (*2*) Eq. (12) with correction for curvature $a = 9.15$ and $b = 0.12$. The data are taken from [83]

molecules grafted onto the surface of CNTs. For example, in [86], double-wall CNTs (with an admixture of single-, three- and multi-wall CNTs), which were initially treated with acid, reacted with diamines: 1,12-diaminododecane (1), 7,10-trioxa-1,13-tridecanediamine (2) and 4,4′-(4,4′-methylene-bis(4,1-phenylene)-bis(methylene))-dianiline (3). Epoxy nanocomposites containing 0.1 wt.% of double-wall CNTs had the following values of the shear modulus G' ($T < T_g$): 989 (1), 993 (2), and 1393 MPa (3), whereas for the matrix $G' = 731$ MPa.

In [55], functionalization of halloysite nanotubes was carried out using 3-(2-aminoethyl)-aminopropyltriethoxysilane, (3-glycidyloxypropyl)-trimethoxysilane or octyltriethoxysilane to produce grafted amino and epoxy groups and a functionless "tail." The corresponding composite materials containing 2.5 or 5.0 wt.% of the above NPs had $G'(50)$ and $G'(200)$ at or slightly higher than the initial matrix, while T_g did not change (173–176 °C).

According to general ideas, functionalization facilitates the dispersion of nanotubes in a matrix. For example, according to [87], amino-functionalized CNTs have higher surface energy than unmodified CNTs, and their wettability with epoxy resin is much better, and grafted amine molecules resulting from functionalization efficiently inhibit CNT re-agglomeration during resin curing. However, functionalization also enhances adhesion at the CNTs/epoxy resin interface, thereby improving the mechanical properties of the matrix. Essentially, the problem is reduced to the formation of an interfacial layer (see the previous section) and its role in controlling the properties of the composite material.

Using scanning electron microscopy (SEM), N. Lachman and H.D. Wagner [88] studied the fractured surfaces of epoxy nanocomposites after stretching MWCNTs. The diameter of a footprint from the removed tube was regarded as a marker of epoxy adhesion. It was found that the diameter of the unmodified MWCNTs is slightly larger than the diameter of the nanotubes, whereas in the case of carboxyl- and amino-functionalized MWCNTs, the diameter of the footprint is several times larger. These data are consistent with the results of mechanical testing of nanocomposites.

Thus, the formation of the interfacial layer is responsible for the reinforcement of nanocomposites.

Moreover, when analyzing the effect of low concentrations of the filler, it is impossible not to take into account the contribution of the matrix to the mechanical properties of composites, whose structure changes due to the effect of NPs on its formation. The catalytic effect of surface groups leads to a frontal autocatalytic reaction, which results in a heterogeneous microphase structure of the polymer (Fig. 5) [89].

Due to the existence of areas with different packing densities in the polymer (this prevents the crack propagation under loading), the energy of viscous destruction increases, elongation at break increases, and, accordingly, the strength of the samples increases. Therefore, it is obvious that the classical additivity formulas are of limited use for calculating the physicomechanical parameters of nanocomposites.

Two-dimensional fillers: Graphene and MMT

For 2D sheets, the aspect ratio χ should also be considered as the ratio of diameter to thickness. The authors of [90] developed a method (references in [90]) to estimate the value of χ from the viscosity of dilute suspensions according to the Einstein eq. (14):

$$\eta_r = 1 + k_1\phi, \tag{14}$$

where η_r is the relative viscosity, ϕ is the volume fraction of suspension ($\phi < 0.02$), and coefficient

$$k_1 = \frac{\chi}{2\ln(2\chi) - 3} + 2. \tag{15}$$

The authors investigated two types of graphene, which were obtained using different technologies. The elastic modulus of the composite material was calculated using Eq. (12), except that formula (4) was modified to (16):

$$E_c = \frac{1}{5}E_{11} + \frac{4}{5}E_{33} \tag{16}$$

and $E_{11} = E_{22}$ and E_{33} were obtained through the expression (12). It was assumed that $\chi = 2$ for E_{33}, and the value of χ is a fitting parameter for E_{11}. E_f was calculated by the formula (16), where E_{f11} was in the range of 250–1000 GPa and E_{f33} = 50 GPa.

Figure 6 presents the results of mechanical testing of graphene-based epoxy nanocomposites [90]. As is clear, these data are satisfactorily described by Eq. (12). The fitting value $\chi = 1000$ is close to the value calculated from the rheological measurements: ~1250.

X. Wang et al. [91] investigated the effect of graphene size on the mechanical properties of an epoxy nanocomposite (Fig. 7). GO samples 1, 2, and 3 had the conditional sizes of 10.79, 1.72 and 0.70 μm.

It is known that in the case of CNTs, the smaller the diameter, the stronger the effect [60]. This is primarily due to the fact that the value of the specific surface is inversely proportional to the radius. However, for 2D graphene sheets this ratio is absent.

In fact, as shown in Fig. 7a, the elastic modulus of the composite is almost insensitive to the size of the filler. As for fracture toughness, the situation is different (Fig. 7b): the stress concentration coefficient K_{1c} increases with decreasing size. K_{1c}, associated with the size of graphene NP, is critical

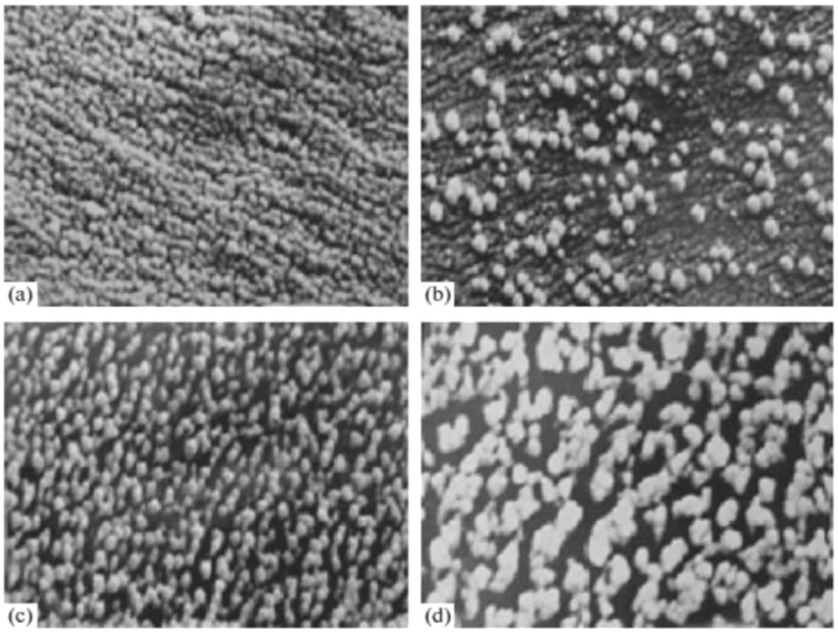

Fig. 5 SEM photographs of epoxy composites with content of carboxylated MWCNTs of (**a**) 0, (**b**) 0.01, (**c**) 0.10, and (**d**) 0.5 wt.%. Magnification of 20,000×. The data are taken from [89]

for increasing toughness. Graphene sheets in an epoxy matrix disturb the crack propagation and prevent their expansion. According to [91], they behave like bridge particles, which serve as rods connecting the crack faces. Therefore, their significant concentration (the smaller the particle size, the higher the numerical concentration) becomes of importance.

As was shown in [92], graphene is more effective than CNTs to improve the mechanical properties of epoxy nanocomposites. For example, at a concentration of 0.1 wt.%, the value of K_{1c} increases by 14% for SWCNTs, by 20% for MWCNTs and 53% for graphene compared to the matrix. Comparative data on tensile testing of epoxy nanocomposite with MWCNTs and graphene are given in Table 1 [93]. It is seen that graphene stiffens the composite to a greater degree than MWCNTs: the modulus is higher and the strength is lower in correlation with a decrease in elongation before breaking.

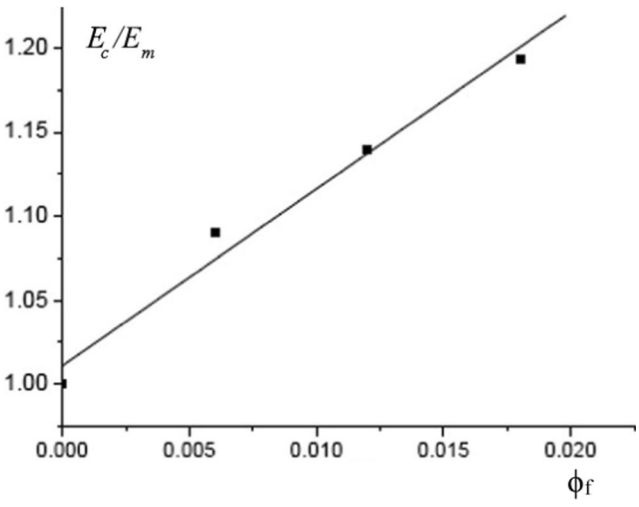

Fig. 6 Dependence of the elastic modulus of the epoxy nanocomposite on the concentration of graphene. Points refer to experiments, and the straight line refers to Eq. (12), where $E_{f11} = 1000$ GPa and $\chi = 1000$. The data are taken from [90]

In general, in the case of polymer nanocomposites, graphene is superior to CNTs in terms of rheological, thermal, and mechanical properties. This circumstance can be explained by the two-dimensionality of graphene and its higher specific surface. As a result, in the case of graphene, the interfacial zone is more extensive, and the interfacial interaction of the filler with the polymer matrix is stronger, whereas interfacial CNTs can interact with polymers only through 1D linear contacts [94].

X. Tang et al. [95] used triglycidyl-*p*-aminophenol as an agent for the transfer of graphene oxide NPs from water to BADGE. Triglycidyl-*p*-aminophenol is adsorbed on the surface of GO, and its sheets exfoliate without any other chemical treatment and randomly distributed in the epoxy matrix. In addition, triglycidyl-*p*-aminophenol is an efficient modifier of the GO surface enhancing interfacial interaction in the composite. As a result, the mechanical properties of epoxy nanocomposites are improved (Table 2). It is seen that the filler itself contributes to an increase in modulus, but the strength decreases in correlation with decreasing elongation at break (lines 1, 2). In the presence of triglycidyl-*p*-aminophenol, all parameters, including ε, grow (lines 3, 4, 6). Lines 6–8 demonstrate that the dependence of the mechanical properties of the epoxy nanocomposite on the GO concentration follows a nonmonotonic pattern, with the optimal component being 1%. In [96], graphene was obtained from graphite powder by a chemical method and then functionalized with a mixture of 4-aminobenzoic and polyphosphoric acids. The epoxy nanocomposites contained 1 wt.% graphene.

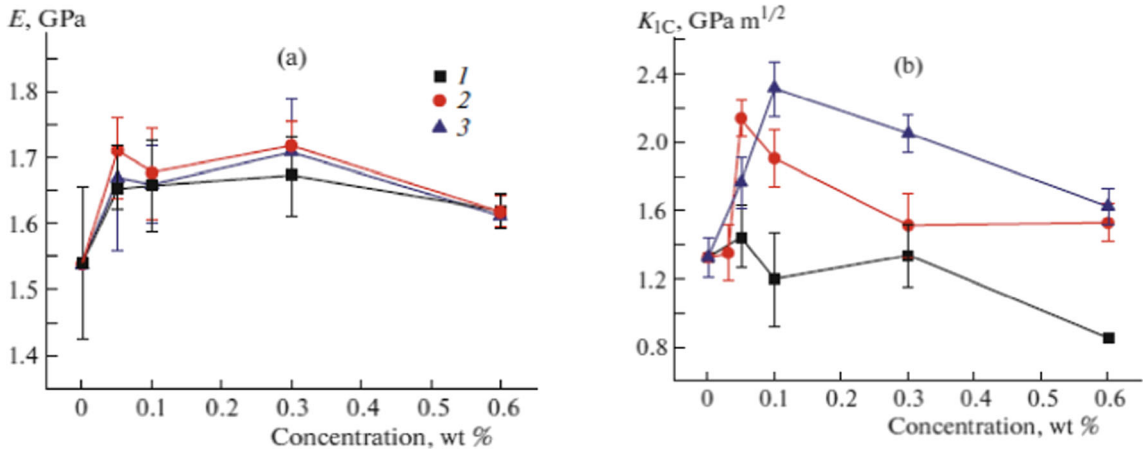

Fig. 7 Dependence of (a) elastic modulus and (b) fracture strength on concentration. The sizes of graphene NPs are (*1*) 10.79, (*2*) 1.72, and (*3*) 0.70 μm. The data are taken from [91]

Figure 8 shows the relaxation characteristics measured at a frequency of 1 Hz, as well as the values of *G*' and tan δ for the matrix and epoxy nanocomposites containing neat and amino-functionalized graphenes. As can be seen, at temperatures below T_g, the modulus of the composites the with the matrix, and the functionalization provides a more pronounced increase in *G*'. As follows from the measurements of tanδ, T_g shows the same trend.

In [97], the mechanical properties of epoxy nanocomposites were improved by the amino functionalization of graphene NPs, which was performed by treating its COOH modification with butadiene and acrylonitrile copolymer containing terminal amino groups. As for the module, a slight increasing effect was observed (Fig. 9a). On the contrary, the fracture toughness increased significantly with filling, especially in the case of amino-functionalized graphene (Fig. 9b).

GO has a chemically active surface due to the presence of hydroxyl, carboxyl, carbonyl, and epoxy groups [98]. This circumstance allows us to expect that GO will demonstrate reinforcing abilities. In addition, GO can be functionalized through the reaction of these groups. In [62], GO was modified with 3-glycidoxypropyltrimethoxysilane, while the authors [63] used BADGE for this purpose. Table 3 lists the mechanical properties of the epoxy matrix and the corresponding composites. It is clear that the epoxy polymer becomes rigid after the addition of GO, and the functionalization of GO enhances this effect. Low concentration of additive is used. As the concentration increases, the modulus increases, but the strength decreases, which correlates with a decrease in elongation at break. This trend seems typical [82].

Table 1 Mechanical properties of reinforced nanocomposites: Young's modulus *E*, breaking stress σ, and elongation at break ε [93]

Material	Concentration (wt.%)	*E* (GPa)	σ (MPa)	ε (%)
Matrix	0	1.63	59	5.9
MWCNTs	0.25	1.95	68	5.4
	0.50	2.00	69	4.8
	0.75	2.27	72	4.9
	1.50	2.04	75	5.7
Graphene	0.25	2.16	65	4.3
	0.50	2.30	64	3.8
	0.75	2.39	68	3.7
	1.50	2.47	69	3.7

Y. Ni et al. [99] managed to overcome this trend when they developed 3D framework consisting of GO sheets. An aqueous solution of poly(amide amine) (dendrimer) was mixed with the GO suspension in a 1: 1 weight ratio. This mixture was quickly frozen in liquid nitrogen and lyophilized. Heating the resulting porous body at 150°C resulted in amidation and reduction of GO. As a result, a three-dimensional graphene product (3DG) with a specific surface area of ~200 m^2/g was produced and used to reinforce the epoxy matrix.

Figure 10 shows the stress-strain curves of the matrix and epoxy nanocomposites with GO and 3DG. The modulus and strength of the composites (curves *2–4*) are higher than those of the matrix (curve *1*), while the final elongation is lower. When GO is used as a filler, the mechanical parameters are better by 0.1% (curve *3*); their deterioration by 0.2% (curve *2*) corresponds to the above trend. The best parameters are observed for a composite with a 3DG filler with a concentration of 0.2% (curve *4*).

As shown in [100], optimal mechanical properties (ultimate tensile strength, ultimate flexural strength, impact resistance and fracture toughness) of an epoxy nanocomposite with MMT additives were achieved at 3 wt.% and corresponded to an increase in these characteristics by 41, 20, 95 and 19% compared to the matrix. This result was explained and confirmed by exfoliation of MMT, studied by X-ray diffraction.

Analogous data were reported by M. Wang et al. [101]. Young's modulus, ultimate strength and elongation at break,

Table 2 Mechanical properties of epoxy nanocomposites with GO [95]

Line number	Material	Concentration of GO (wt.%)	Concentration of triglycidyl-*n*-aminophenol (wt.%)	*G*' (30 °C), GPa	σ (MPa)	ε (%)
	Matrix	0	0	2.06	53	5.4
1	Epoxy nanocomposite	0.5	0	2.26	51	4.8
2		1.0	0	2.34	46	4.2
3		1.0	5	2.67	57	4.3
4		1.0	10	2.75	66	4.8
5		0	20	2.12	51	4.4
6		0.5	20	2.58	82	5.7
7		1.0	20	2.94	101	6.2
8		1.5	20	2.84	83	5.0

as well as K_{1c} of an epoxy nanocomposite had maximum values at an MMT concentration of 1 wt.%. These values are higher than the corresponding matrix parameters by 5, 38, 64, and 93%, respectively.

In accordance with [87], the addition of 3 wt.% of NPs of MMT, SiO_2 or their mixture (1:1, *w*/w) affects the mechanical properties of the epoxy nanocomposite (Table 4) [102]. The addition of SiO_2 significantly increases the fracture toughness K_{1c} and tensile strength σ, but the ultimate elongation ε grows slightly. This conclusion indicates a tightening of the matrix. The introduction of MMT, in contrast, increases ε and σ, but K_{1c} slightly increases. All of these parameters increase markedly when MMT + SiO_2 mixed NPs are added. Apparently, the difference in the efficiencies of fillers is explained by their various shapes.

In fact, SiO_2 are spherical particles, MMT are sheets with an aspect ratio of ~1000, and mixed NPs have a complex shape in the form of sheets with attached balls. If the main mechanism of nanocomposite destruction is associated with the propagation of cracks by exfoliating the matrix of NPs, then the synergistic effect of the mixed filler becomes clear. In this filler, a very complex surface profile determines the elongation of the crack propagation path and the increase in the energy of composite destruction.

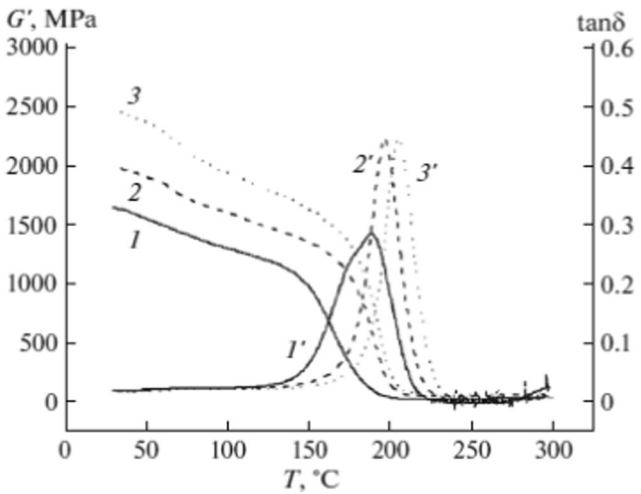

Fig. 8 Real modulus *G*′ (*1*–*3*) and tan δ (*1*′-*3*′) of the matrix (*1*, *1*′) and nanocomposites with the original (*2*, *2*′) and functionalized (*3*, *3*′) graphene. The data are taken from [96]

Three-dimensional fillers: Fullerene and metal-containing compounds

Fullerene is of interest as a nanofiller of epoxy nanocomposites, since, unlike other carbon components, CNTs and graphene, it is 3D (often fullerene is considered as a 0-dimensional object), and its aspect ratio is one. Papers on the bonds of epoxy nanocomposites with fullerene filler are few [103–105]. But in all cases the observed trend is as follows: the modulus is weakly sensitive to filling (Fig. 11); however, even at low fullerene concentrations, the strength parameters of the composite increase significantly.

For epoxy nanocomposites, the main ways to resist destruction are the introduction of particles that can act as rods connecting the crack faces in the matrix. and the extension of the crack propagation path through branching caused by encountering NPs and/or its propagation through exfoliation of the matrix. Fullerene particles meet the requirements of these mechanisms due to the high energy of interaction with the chain fragments of the epoxy matrix and high numerical concentration. When a crack interacts with obstacles, its elongation occurs steadily, without destruction of the body in a significant load range.

As was shown above, metal-containing NPs should be divided according to the method of their formation: whether they were pre-formed, mixed with a binder and cured in their presence or formed in situ during the formation of epoxy nanocomposites. Metal oxides are of the first type, while metals are mainly of the second type. Depending on the synthesis conditions, the particles of metal oxides have different morphologies and sizes. For example, NPs of iron oxides

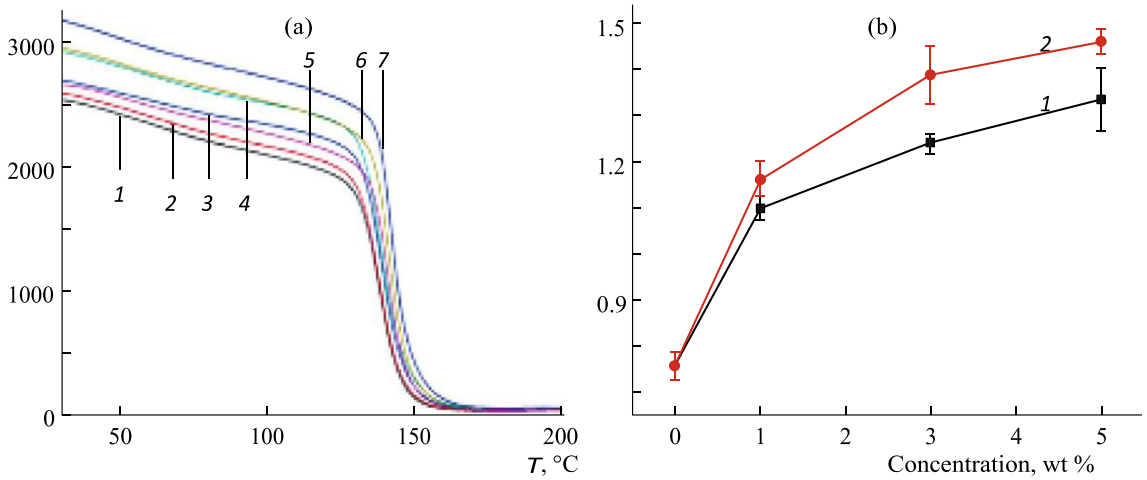

Fig. 9 **a** Temperature dependence of the real modulus (at a frequency of 1 Hz) of the epoxy matrix (*1*) and nanocomposites with original (*2–4*) and NH_2-functionalized (*5–7*) graphene. Concentrations are (*2*, *5*) 1, (*3*, *6*) 3, and (*4*, *7*) 5 wt.%; (**b**) dependence of the fracture strength of nanocomposites with original (*1*) and NH_2-functionalized (*2*) graphene on concentration. The data are taken from [97]

F_3O_4, synthesized in the presence of triethanolamine or urea surfactants, are polygonal or elongated in shape, and their average sizes are ~18 or ~39 nm [106]. Accordingly, the properties of epoxy nanocomposites filled with these particles were different.

Figure 12 shows stress-strain curves for the epoxy matrix (curve *1*) and epoxy nanocomposites containing 1 wt.% of polygonal (curves *2*, *3*) and elongated (curve *4*) F_3O_4 NPs. The last two particles (*3*, *4*) were treated with 3-aminopropyl-trimethoxysilane. As follows from the above data, fillers have little effect on the structure of the polymer, since the value of modulus is almost the same for the matrix and composites. At the same time, the strength increases markedly, and treatment with aminosilane helps in this trend (curves *2*, *3*). Elongated NPs reinforce composites more efficiently than polygonal NPs (curves *3*, *4*). The value of fracture toughness K_{1c} varies in the same sequence: 0.11, 0.43, 0.62, and 0.89 MPa·$m^{1/2}$.

The efficiency of functionalization of metal oxide NPs was confirmed by the data [107], in which cubic Fe_2O_3 particles with a size of ~40 nm were treated with 3-aminopropyl-trimethoxysilane. The results are summarized in Table 5. As can be seen, the strength of the composites is increasing compared with the matrix. However, the increase in fracture toughness is provided exclusively by functionalized NPs.

I.A. Al-Ajaj et al. [108] investigated how the size of filler particles affects the mechanical properties of epoxy composites using TiO_2 as an example. Nanocomposites (NPs with a size of ~50 nm) and microcomposites (particles with a size of ~50 μm) were compared. The results of three-point bending tests are shown in Fig. 13. Up to a concentration of 4%, NPs increase all the mechanical characteristics of the composite (Fig. 13, curves *1*). Further reduction is likely due to the increase in particles due to their agglomeration. In the case of microparticles, the modulus increases with increasing concentration (Fig. 13b, curve *2*), and the strength parameters deteriorate (Fig. 13a, c, curves *2*). This seems to indicate that the coarse particles act as stress concentrators. This circumstance

Table 3 Mechanical properties of epoxy nanocomposites with modified GOs [62, 63]

Material	Concentration (vol.%)	*E* (GPa)	σ (MPa)	ε (%)	K_{1C} (MPa·$m^{0.5}$)
Matrix	0	3.15	53	3.75	0.50
GO	0.10	3.27	72	4.23	0.59
	0.25	3.32	68	3.85	0.63
	0.50	3.36	65	3.51	0.63
BADGE-functionalized GO	0.10	3.35	95	6.45	0.68
	0.25	3.56	93	6.32	0.71
	0.50	3.67	85	5.86	0.67
Silane oxide-functionalized graphene	0.10	3.32	81	–	0.69
	0.25	3.46	79	–	–
	0.50	3.60	72	–	–

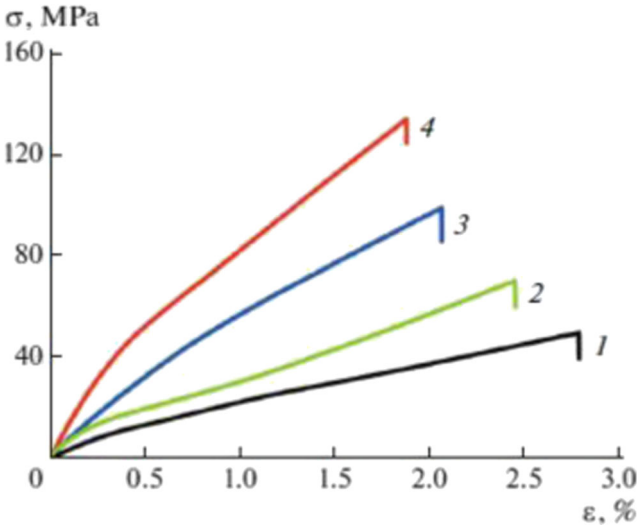

Fig. 10 Stress-strain curves of the matrix (*1*) and the epoxy nanocomposites with GO (*2*, *3*) and 3DG (*4*). Concentrations are (*2*, *4*) 0.2 and (*3*) 0.1 wt.%. The data are taken from [99]

is favorable for the destruction of the material. At the same time, at low concentrations, NPs increase the strength of epoxy nanocomposite by interacting with cracks, as described above.

An example of epoxy nanocomposites with fillers formed in situ is given in [109]. It was shown that the dependences of the Young's modulus *E*, the breaking strength σ and the elongation ε on the concentration of the precursor, silver myristate, are described by extreme curves with a maximum corresponding to 0.09 wt.%. This result contrasts sharply with the data presented in the previous paper, where the maximum parameters correspond to 4 vol.%, i.e., more than two orders of magnitude higher. Perhaps this is due to the size of NPs: in the case of Ag, the average NP radius is 8.7 nm; for TiO_2, 25 nm.

Electrophysical properties

For the electrophysical properties of epoxy nanocomposites, the percolation threshold, which depends on the volume concentration, spatial distribution and aspect ratio of NPs, plays a decisive role along with the electrophysics of the fillers.

Table 4 Mechanical properties of epoxy nanocomposites with MMT/SiO_2 [102]

Material	σ (MPa)	ε (%)	K_{1C} (MPa·m$^{0.5}$)
Matrix	58.2	0.49	0.52
Epoxy nanocomposite/SiO_2	87.4	0.76	0.93
Epoxy nanocomposite/MMT + SiO_2	94.9	2.91	1.06
Epoxy nanocomposite/MMT	87.4	3.70	0.56

The percolation threshold

The percolation theory [110] is based on the idea that as the volume concentration ϕ increases, NPs are combined into ever-increasing clusters and, when a certain value of ϕ_c is reached, they form an infinite structure called a percolation cluster. The value of ϕ_c is the percolation threshold. If NPs are able to conduct electricity, namely at $\phi \geq \phi_c$, the electrical conductivity σ of the composite increases by orders of magnitude. Increases change in σ appears as a sharp increase in a narrow range of NP concentrations. This allows percolation transition insulator-conductor to be considered as a second-order phase transition.

All clusters have a fractal structure. The "journey" along the bonds connecting NPs in the final cluster ($\phi < \phi_c$) inevitably leads to terminal branches ("tails"). A percolation cluster ($\phi \geq \phi_c$) has, if only one center connects the opposite borders of the composite sample, although the number of "tails" in its structure is more than enough. In the vicinity of the percolation threshold, the dependence σ(ϕ) is described by relations (17):

$$\sigma \propto \begin{cases} 0, & \phi < \phi_C \\ (\phi - \phi_C)^{\beta}, & \phi \geq \phi_C \end{cases} \quad (17)$$

For convenience of further presentation, it is useful to introduce the idea of the correlation length (characteristic size) of the final cluster ξ, (18):

$$\xi \propto (\phi_c - \phi)^{-\nu}, \quad \phi < \phi_C \quad (18)$$

The parameters β and ν are called critical parameters.

Naturally, the percolation threshold depends on the structural characteristics of NPs. Figure 14 presents data reported by J. Li et al. [111] on the influence of the degree of dispersion and the aspect ratio χ of particles on the value of ϕ_c. These authors considered the behavior of cylindrical NPs with a length *l* and a diameter *d* and came to the equation came to $\phi_c = f(\chi)$, reaching a plateau and only aggregation becomes the decisive factor. The lower the aggregation, i.e., the higher the dispersion of particles, the lower the percolation threshold. At the same time, as follows from these data, the value of ϕ_c is insensitive to the size of NPs at $\chi < 10$. Experimental data on MWCNTs are also presented in the Figure as open circles [111].

The value of the critical concentration ϕ_c depends not only on such parameters as the size and shape of NPs but also on the interaction between them and the matrix. This point can be illustrated by the data [112] shown in Fig. 15. If for non-functionalized MWCNTs the percolation threshold estimated by electrical conductivity is less than 0.1% (curve *1*), then the

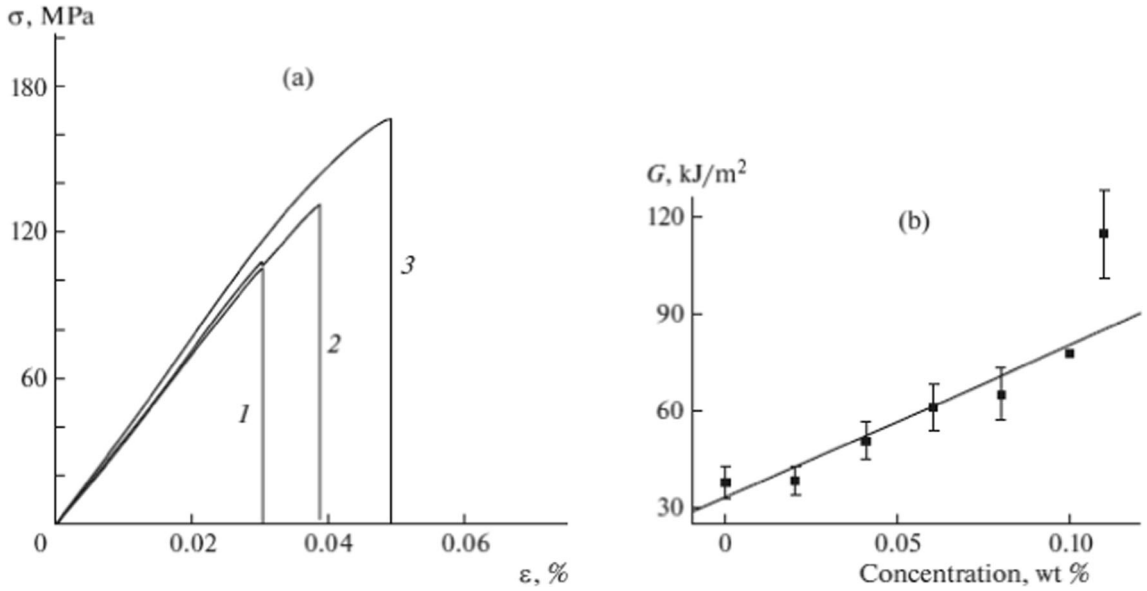

Fig. 11 Stress-strain curves of the matrix and epoxy nanocomposite (**a**) and the dependence of shock strength of epoxy nanocomposite on the concentration of fullerene (**b**). (a) Concentrations of fullerene are (*1*) 0, (*2*) 0.04, and (*3*) 0.1 wt.%. The data are taken from [104]

introduction of COOH groups that drastically change the nature of interaction of the tubes with the matrix shifts ϕ_c to the right (curve *2*).

These findings were tested in [113], in which the authors compared chemically equivalent compounds and suggested that covalent functionalization, which is favorable with respect to the mechanical properties of the composite material, does not improve its conductive characteristics in any way.

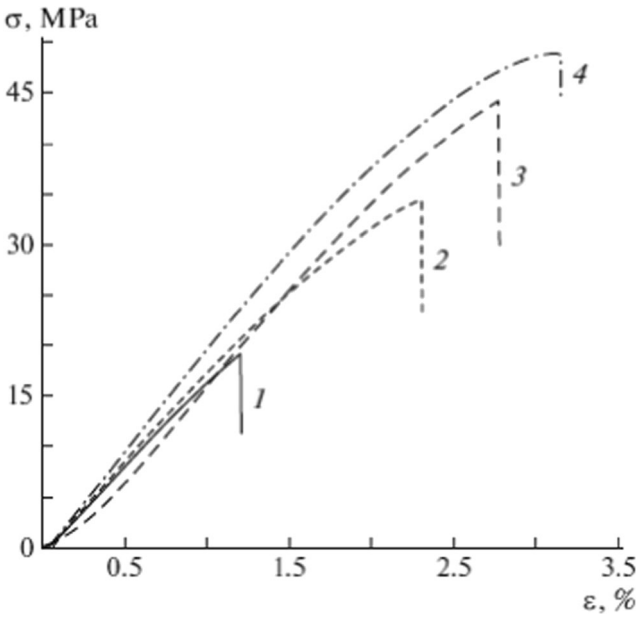

Fig. 12 Stress-strain curves of the matrix (*1*) and the epoxy nanocomposite with polygonal (*2*, *3*) and elongated (*4*) F_3O_4 NPs treated with 3-aminopropyltrimethoxysilane. The data are taken from [106]

Electrical conductivity of epoxy nanocomposites with carbon nanoparticles

CNTs and graphene are anisodiametric particles; therefore, the electrical conductivity of polymer composites will be determined by their aspect ratio, the pattern of orientation, and degree of dispersion. These parameters will determine the value of the percolation threshold.

The electronic and, therefore, conductive properties of CNTs depend on their chirality. The latter appears during synthesis and characterizes the method of twisting the graphene plane into the cylinder. The diameter and helicity of the tube are associated with chirality. Limiting cases are found in zigzag and chair configurations. The first structure is completely symmetric (zero chirality), and the second structure is helical at an angle of 30°.

SWCNTs with zigzag structure are semiconductors, while their chair-type structures are conducting. MWCNTs are always conductors. Macroscopic samples of SWCNTs in the form of randomly arranged bundles are characterized by conductivity up to 10^3 S/cm. However, the specific resistance of the system is determined not so much by the properties of CNTs as by the contacts between them; that is, the limiting stage of conductivity occurs through the hopping mechanism [114].

Charge carriers of graphene behave like massless relativistic particles (Dirac fermions). High electrical conductivity in a layer is associated with a high quality of its crystal lattice, i.e., with a low concentration of various types of defects that act as scattering sites and types charge transfer by limiting the electron free path length [115]. Although graphene has a higher electrical conductivity compared to MWCNTs (~10^6 vs.

Table 5 Mechanical properties of epoxy nanocomposites with Fe_2O_3 [107]

Material	Concentration (wt.%)	σ (MPa)	K_{1C} (MPa·m$^{0.5}$)
Matrix	0	59.3	1.21
Epoxy nanocomposite without Fe_2O_3	1	63.2	1.19
	2	67.8	1.16
Epoxy nanocomposite functionalized with Fe_2O_3	1	73.6	1.88
	2	78.3	2.06
	3	84.8	2.27
	4	89.1	2.49

~10^5 S/cm), the percolation threshold of the latter in polymer composites is much lower: mass percent fractions vs. 1–2% [94, 116].

The electrical conductivity of composites is usually studied by analyzing the concentration and temperature dependences of dc conductivity σ_{dc} (dc measurements) and the real part of complex ac conductivity σ_{ac} (ac measurements). The data presented in [112] illustrate the first approach (see Fig. 15). The second approach was implemented by A. Vavouliotis et al. [117] in the study of the electrical conductivity of epoxy nanocomposites, in which MWCNTs were used as NPs. The results are shown in Fig. 16.

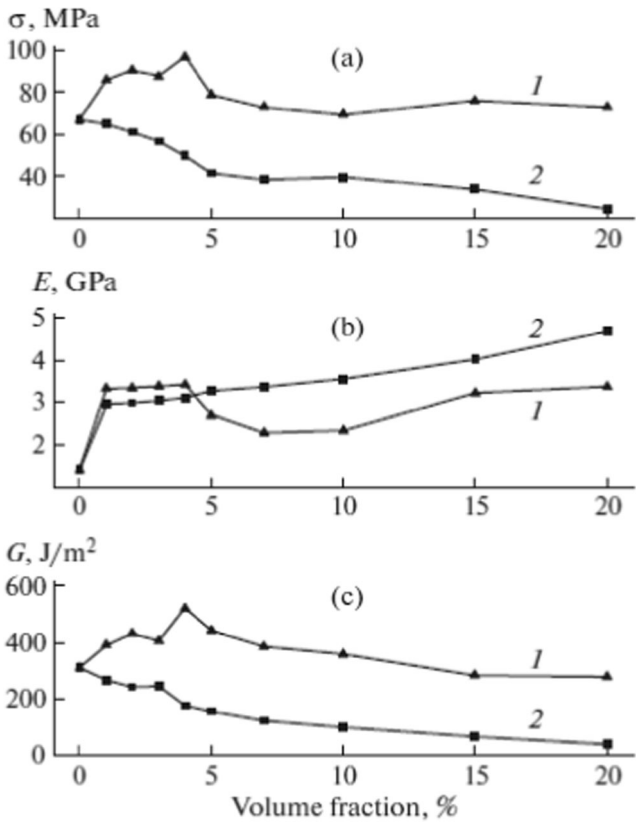

Fig. 13 Dependence of (**a**) strength, (**b**) modulus, and (**c**) fracture energy of the composite on the volume fraction of (*1*) NPs and (*2*) microparticles of TiO_2. The data are taken from [108]

It can be seen that σ_{ac} depends on the frequency and content of MWCNTs and grows by almost ten orders of magnitude with an increase in these values. The curves of ac conductivity of the matrix and the sample with the lowest concentration almost coincide and show a power-law dependence of σ_{ac} on ω. In the low-frequency range, there is a sharp increase in conductivity (up to eight orders of magnitude) between samples containing 0.1 and 0.3 wt.% MWCNTs. Nanocomposites with concentrations equal to or greater than 0.3% demonstrate a broad plateau of the so-called apparent dc conductivity. Apparently, the percolation threshold clearly demonstrates itself.

Based on the dc conductivity data and using Eq. (17), the critical concentration of MWCNTs ϕ_c and the critical factor β were estimated as 0.089 wt.% and 2.574, respectively. For ac conductivity, the results were as follows: $\phi_c = 0.098$ wt.% and $\beta = 3.204$.

This difference can apparently be explained by different conductivity. The dc conduction is determined via overcoming energy barriers between favorable conductive areas within

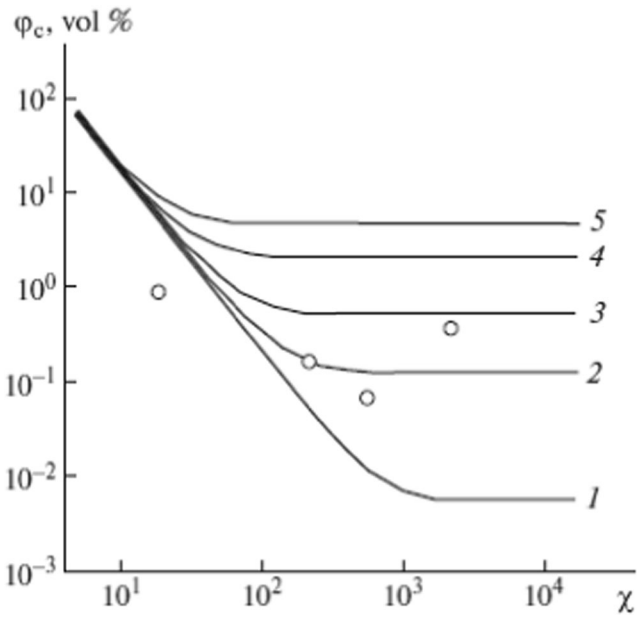

Fig. 14 Relation of the value of ϕ_c to parameters χ and ε. ε = (*1*) 0.01, (*2*) 0.05, (*3*) 0.1, (*4*) 0.2, and (*5*) 0.4. See text for explanations. The data are taken from [111]

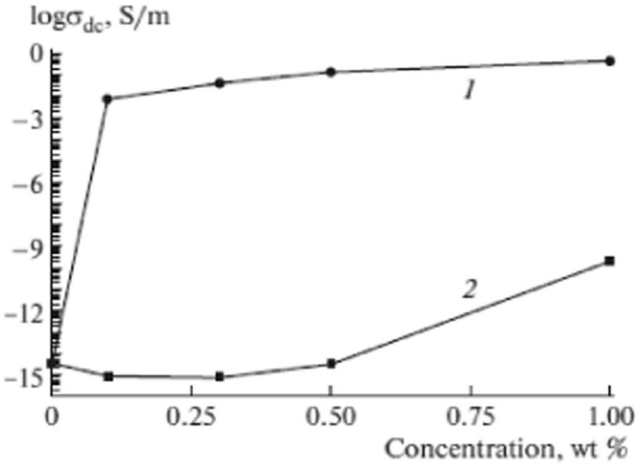

Fig. 15 Dependence of dc conductivity of the epoxy nanocomposite on the concentration of (*1*) original and (*2*) COOH-functionalized MWCNTs. The data are taken from [112]

the material and forming a continuous percolation path between the electrodes. Charge carriers are forced to migrate over long distances. In addition, with ac conduction, an increase in frequency leads to a decrease in the average shift of current carriers and an increase in σ_{ac}, since a better use of conductive particles is achieved. The probability of hopping conduction between the latter increases, and the conductivity includes contributions from both the continuous path and the existing terminal branches. Thus, when ac measurements, any contact resistances are eliminated and/or reduced at all scale levels of the interaction (from samples of macroelectrodes to nanotubes-nanotubes).

G.D. Seidel and D.C. Lagoudas [118] developed a model to evaluate the effect of electron hops and the formation of conductive circuits in the electrical conductivity of CNT-polymer nanocomposites by using conductive interfacial layer. If well-dispersed CNTs are located in close proximity, then the hops of electrons can occur easily. The critical thickness of the interlayer that provides a hopping mechanism of conduction does not depend on the diameter (*d*) of tubes. Note that the above *d*, the more pronounced the percolation concentration. For MWCNTs, the radius is higher than SWCNTs, so that the percolation threshold that is associated with a hopping of electrons is much higher. In fact, as was found in the [119] in the epoxy nanocomposites with SWCNTs, ϕ_c is about 0.015 wt.%; in the case of the CNT mixture, ϕ_c is about 0.0225.

At high concentrations, the conductivity of the composite material will be determined by the electronic properties of the CNTs. But if MWCNTs are conducted, then a certain proportion of SWCNTs are semiconductors. Therefore, at equal concentrations, the SWCNTs will have lower electrical conductivity than the MWCNTs. In this case, the electrical conductivity will be $\sim 10^{-5}$ and $\sim 10^{-6}$ S/cm, respectively.

The inclusion of conductive NPs in a polymer medium dramatically changes its dielectric parameters, which in the alternating electric field are characterized by complex dielectric constant ε*, or permittivity (19):

$$\varepsilon^* = \varepsilon' - i\varepsilon'' \tag{19}$$

where ε′ and ε″are the real and imaginary parts of the dielectric permittivity. The first value is a component of polarization that changes in phase with a variable field, and the last value is a contribution to polarization with a phase shift by π/2 relative to the field and characterizes the dielectric losses.

As shown in [120], the dependence ε′(ϕ) can be described by the same relation as the electrical resistance, namely by Eq. (17): $\phi_c = 0.006$ (0.6 wt.%) and $\beta = 3.7$. The value of ε″ first increases to a critical concentration, and then decreases. Eq. (18) is applicable to the growing branch of the dependence ε′′(ϕ): $\nu = 0.47$.

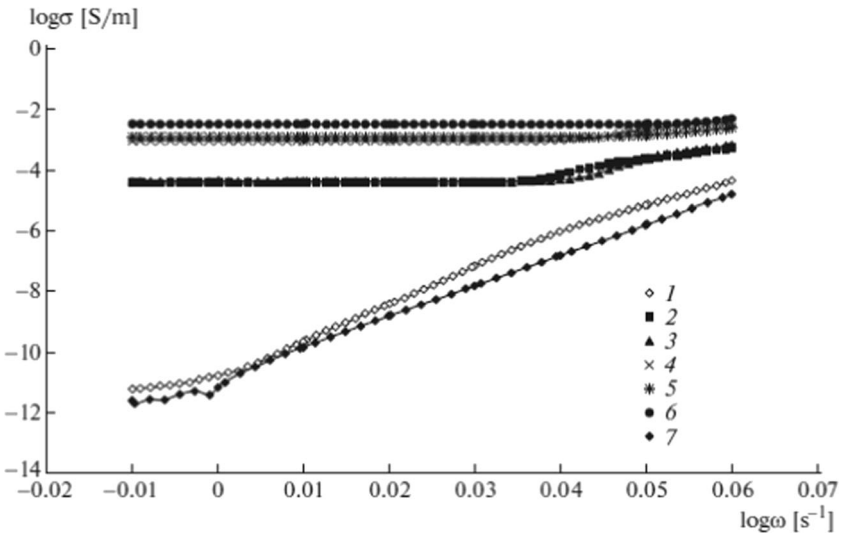

Fig. 16 Dependence of ac conductivity of the epoxy nanocomposite on frequency. The concentrations of MWCNTs are (*1*) 0.1, (*2*) 0.3, (*3*) 0.5, (*4*) 0.6, (*5*) 0.8, and (*6*) 1.0 wt.%; (*7*) matrix. The data are taken from [117]

Metal-containing nanoparticles

It is obvious that the electrophysical properties of epoxy nanocomposites with metal-containing NPs depend on their conductive ability: conductor (Ag, Cu) or semiconductor (Al_2O_3, ZnO). If in the first case the filler can transfer the conductive properties to the composite, then in the latter case it can only modify dielectrics to a greater or lesser extent.

Semiconductors B. Tsonos et al. [121] used dielectric relaxation spectroscopy to study epoxy nanocomposites with ZnO NPs with sizes less than 100 nm. The conductivity data are presented in Fig. 17.

As follows from the frequency dependence of σ'_{ac} (Fig. 17a), at low frequencies all the curves show a plateau. This corresponds to dc conductivity σ_{dc}. However, its value is small (10^{-9} S/cm). This fact implies the absence of direct current conductivity, and the applied field is compensated by the orientation of the dipoles. Since there are no fundamental differences in the curves describing the matrix and composites, it is clear that in this case we are talking about dipoles belonging to polymer chains. NPs interacting with molecular fragments of the matrix facilitate (ZnO concentrations are 10 and 12%) or make it difficult (3 and 7%) for their orientation relaxation.

The data shown in Fig. 17b confirm this conclusion. The temperature dependence of the dc conductivity is described by the empirical Vogel-Fulcher-Tammann law (20):

$$\ln\sigma_{dc} \propto -\frac{B}{T-T_0} \tag{20}$$

(B and T_0 are empirical constants).

This equation is usually used to describe the relaxation dynamics of the α process in polymers. Constant T_0, which is often interpreted as the temperature of "static freezing" of electric dipoles or the transition to the dipole glass state, is 30–60 K below T_g. Both parameters T_0 and B are associated with the so-called strength parameter D through the ratio $D = B/T_0$. The parameter D is inversely proportional to the value of brittleness m (21), which characterizes the degree of deviation from the Arrhenius dependence,

$$m = \left(\frac{\partial \lg\eta}{\partial(T_g/T)}\right)_{T=T_g} \tag{21}$$

Here η is viscosity.

The kinetic fragility index m depends on the inter- and intramolecular interactions in the system and serves as a measure of the bonds formed during the glass transition [122].

Table 6 shows the Vogel-Fulcher-Tammann constants for the systems of interest [121, 123].

A low value of D and, accordingly, a high value of m mean that the glass transition occurs in a narrow temperature range of about T_g, which is typical of polymers.

Thus, the fact that the parameter D is almost insensitive to the existence of NPs in the composite proves that the epoxy matrix makes a decisive contribution to the electrophysical properties of epoxy nanocomposites.

The electrophysical properties of an epoxy composite with $BaTiO_3$ microparticles (less than 2 μm) were investigated by the method of broadband dielectric spectroscopy [124]. It was shown that the imaginary part M'' of the electric modulus M^*, which is defined as the inverse value of the complex dielectric permittivity

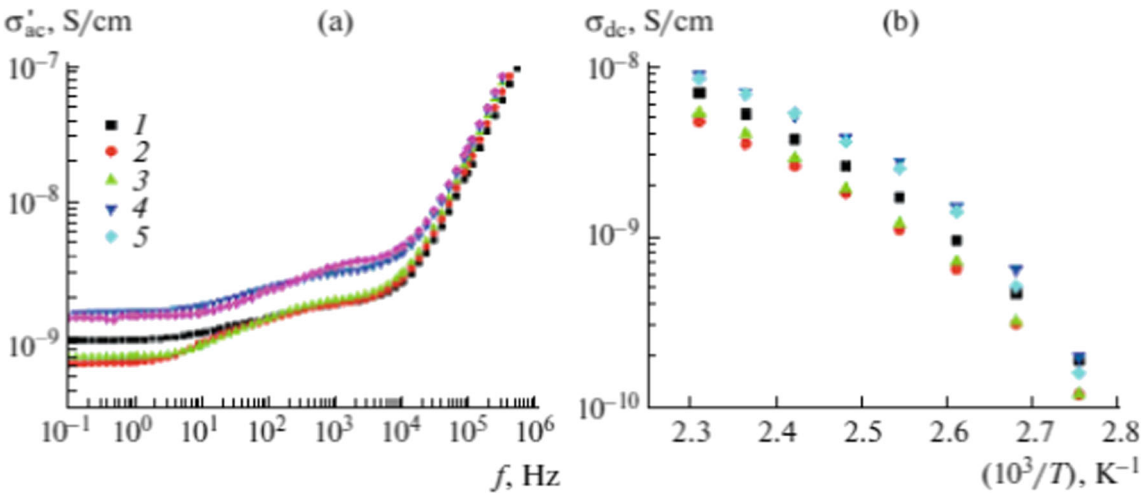

Fig. 17 Dependences of (**a**) specific conductivity σ'_{ac} of the epoxy nanocomposite with ZnO on frequency at 110 °C and (**b**) σ_{dc} of the same composite on temperature at a frequency of 1 Hz. The concentrations of ZnO NPs are (*1*) 0, (*2*) 3, (*3*) 7, (*4*) 10, and (*5*) 12 wt.%. The data are taken from [121]

Table 6 Vogel-Fulcher-Tammann constants for the epoxy nanocomposites with ZnO

ZnO (wt.%)	0	2.9	4.8	6.5	6.5	10.7	Ref.
B, K	714	600	–	699	712	612	109
T_0, K	268	279	–	274	274	276	
D	2.7	2.2	–	2.6	2.6	2.2	
B, K	754	700	675	611	608	550	111
T_0, K	263	268	271	274	278	281	
D	2.9	2.6	2.5	2.3	2.2	2.0	

according to Eq. (22), depends on the $BaTiO_3$ content with a maximum loss that monotonically decreases with the filler concentration:

$$M^* = \varepsilon^{*-1} = (\varepsilon' - i\varepsilon'')^{-1} = \frac{\varepsilon'}{\varepsilon'^2 + \varepsilon''^2} + i\frac{\varepsilon''}{\varepsilon'^2 + \varepsilon''^2} = M' + iM'' \tag{22}$$

The curves *M''(f)* show peaks, which in increasing frequency order can be tied to the interfacial polarization, also known as the Maxwell-Wagner effect; α transition (glass transition); and local β transition, which is usually explained by the rearrangement of the polar side groups of the polymer chains. Figure 18 shows the temperature and concentration dependences of the frequencies f_{max} corresponding to the maxima of the first two peaks.

It can be seen that for all systems the α transition is described by the Vogel-Fulcher-Tammann equation, whereas the interfacial polarization obeys the Arrhenius law. The activation energy for the interfacial polarization process somewhat

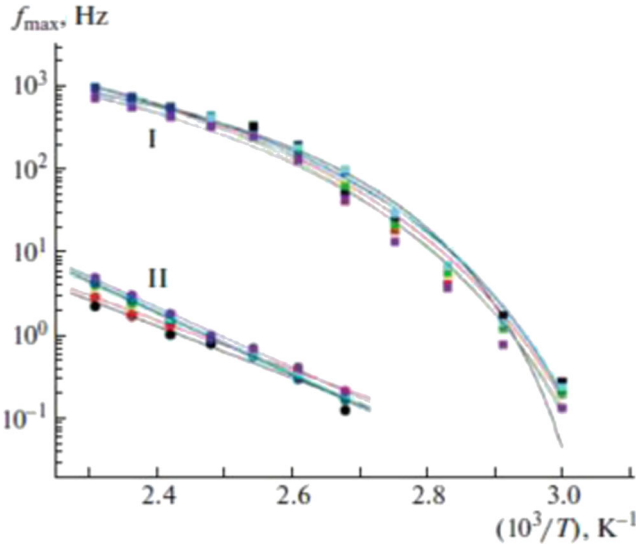

Fig. 18 Temperature and concentration dependences of f_{max} corresponding to (I) the α transition and (II) the interfacial polarization effect. The concentration of $BaTiO_3$ is varied from 0 to 13.6 vol.%. The data are taken from [124]

increases with the content of $BaTiO_3$, but in both cases the dependence on the filler concentration is very weak. Note that interfacial polarization is almost always found in polymers due to the presence of various additives, plasticizers, etc. Parameter T_0 also increases with the filler content in accordance with the increase in T_g.

Consequently, the regularities of the temperature and frequency dependence of *M''* of the composites confirm that the epoxy matrix makes a decisive contribution to the electrophysical properties of epoxy nanocomposites.

S. Singha and M.T. Thomas [125] compared epoxy nanocomposites with TiO_2, Al_2O_3, and ZnO NPs as insulators. The highest efficiency was manifested by TiO_2, which reduced the dc resistance of the matrix from 7×10^{17} to ~2×10^{17} Ω·cm for a composite containing 0.5 wt.% TiO_2. Then ZnO (~3×10^{17} Ω·cm, concentration 0.5 wt.%) and, finally, Al_2O_3 (~4×10^{17} Ω·cm, concentration 5 wt.%) follow. The effect of the filler type on the specific dc resistance of nanocomposites is not very large. Probably, this phenomenon can be explained by the fact that excess free charges are introduced into the composite by particles. The phenomenon is most pronounced in the case of TiO_2.

These fillers have a similar effect on ac dielectric strength. The probability of breakdown was analyzed in terms of the Wiebull distribution (23):

$$F(x) = 1 - \exp\left\{-(x/\lambda)^{\beta}\right\} \tag{23}$$

(λ is the scale parameter, and β is the shape parameter).

The presence of NPs increases the probability of breakdown by a noticeable decrease in the value of λ. For example, λ is 28.6 kV/mm at 0.5% ZnO, while for the matrix λ = 52.3. In the case of Al_2O_3, the scale parameter is 36–40 kV/mm.

Figure 19 shows the ac dielectric strength of epoxy nanocomposites as a function of the concentration and size of ZnO particles [126]. If at low concentrations (less than 10%) the size of NPs has practically no effect, then at high filling (more than 10%) large particles (~500 nm) reduce the electric strength much more strongly than small particles (~65 nm).

Q. Wang and G. Chen demonstrated [127] that the ac dielectric strength of epoxy nanocomposites significantly depends not only on the type of filler, but also on the interfacial layer. For example, the treatment of SiO_2 NPs with silane leads to an increase in λ from 140.1 (matrix) to 151.4 kV/mm, whereas for untreated particles λ = 130.5 kV/mm.

The interfacial layer plays an important role in controlling the properties of composites. However, at low concentration of NPs, their contribution can hardly be determined. Using broadband dielectric spectroscopy, X. Huang et al. [128] studied highly filled epoxy nanocomposites containing 50 vol.% $BaTiO_3$ NPs with six kinds of surface chemistry (Fig. 20). It was assumed that in this case it is the interfacial layers that will

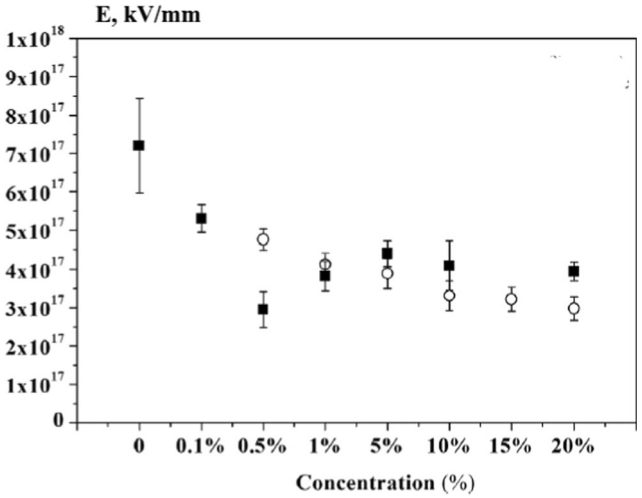

Fig. 19 Dependence of the ac dielectric strength of the epoxy nanocomposite on the concentration of ZnO particles with a size of 65 (closed circles) and 500 nm (open circles). The data are taken from [126]

have a decisive influence on the properties of the composite. In contrast to the dependence constructed, for example, in Fig. 18, in this case the Arrhenius law holds. This means that the matrix does not become apparent. The activation energy (E_a) of conductivity depends on the chemical nature of the groups grafted onto the surface of NPs, i.e., on the structure of the interfacial layer. The lowest values of E_a are manifested by structures formed by amino and epoxy groups that can directly participate in the formation of a matrix network (straight lines *3*, *4*). This is apparently the densest layer. The mobility of the polymer chains is limited, and the dipole or orientation contribution to the polarizability will be minimal.

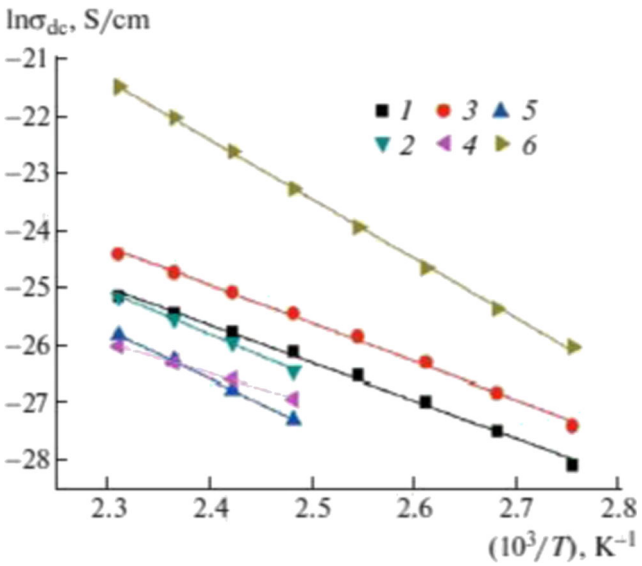

Fig. 20 Temperature dependence of the dc conductivity of the epoxy nanocomposite with $BaTiO_3$ NPs (*1*) without treatment and with (*2*) SH, (*3*) OH, (*4*) NH_2, and (*5*) epoxy grafted groups and (*6*) hyperbranched aromatic polyamide. The data are taken from [128]

The most mobile molecular fragment providing high conductivity is the layer obtained with the participation of hyperbranched aromatic polyamide. The same layer has the highest activation energy (straight line *6*).

Conductors Among conducting metallic NPs, silver is distinguished by excellent electrical conductivity. In [129], epoxy nanocomposites were obtained using Ag powder 70 nm in size. Direct measurements have shown that the dc conductivity is described by the relation (17) at $\phi_c = 1 \pm 0.3\%$ and $\beta = 5 \pm 0.5$. Usually $\phi_c = 15\%$ and $\beta = 2$ [130]. The authors explain this discrepancy of the aggregation of NPs into chain structures with a high aspect ratio; therefore, the percolation threshold is reduced. Another possible reason may be an increase in NPs, but, as shown in [130] (indeed, for microparticles), this leads to a decrease in ϕ_c.

At the same time, ac measurements made in [129] contradict the above data. Figure 21 presents the data on the ac conductivity. As in the case of MWCNTs (see Fig. 16), at low frequencies and rather high concentrations of Ag NPs, curves $\sigma_{ac}(f)$ cease to be frequency dependent, thereby demonstrating the transition to σ_{dc}. However, it can be seen that at concentrations of 2.2 and 3.3% there is no signs of such a trend. The sharp achievement of the plateau corresponds to 8.3%. Therefore, $\phi_c >> 1\%$.

Using Ag powder with a size of 200 nm as a filler, S. Nam et al. [131] showed that, according to measurements of electrical resistance, the percolation threshold is about 0.23. It is interesting to note that the addition of SiO_2 microparticles (1–5 μm) in the amount of 12 vol.% shifts the threshold to ~0.18.

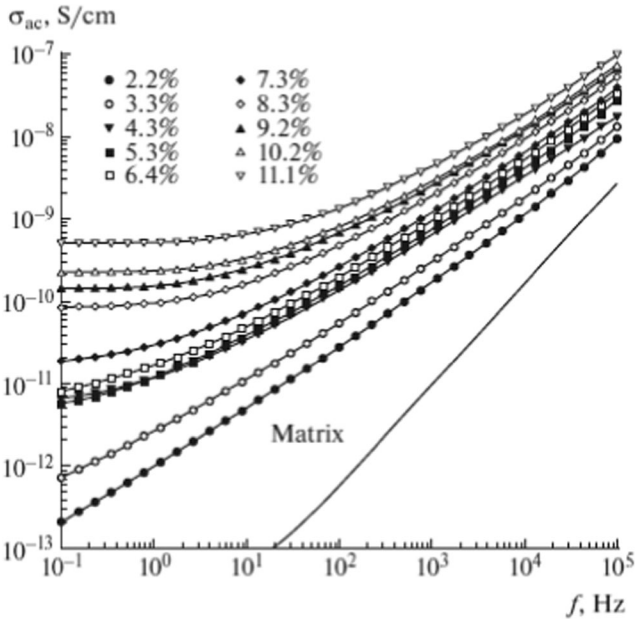

Fig. 21 Frequency and concentration dependences of the ac conductivity of the epoxy nanocomposite with silver NPs. The data are taken from [129]

Based on electron microscopy studies, the authors believe that the supramolecular structure of the matrix becomes more uniform with the introduction of additives.

Further studies [132] showed that the size of SiO_2 particles is of great importance. When 5 vol.% NPs with a diameter of 1000 nm was added, the percolation threshold ϕ_c decreased from 0.23 to 0.14. In the end, NPs with a smaller diameter (500, 80, and 10 nm) reduced ϕ_c to 0.1.

In [133], silver NPs with sizes of 15–20 nm were synthesized in situ by the reduction of $AgSbF_6$. The percolation threshold according to the ac conductivity measurements was not reached even at 20 wt.% precursor; this value corresponded to approximately 5 wt.% or ~0.5 vol.% Ag NPs, which is quite natural.

At filler concentrations higher than ϕ_c, dielectric spectroscopy measurements reflect the relaxation properties of the matrix and the effect of NPs on them. For example, as shown in [134], which is a continuation of the previous study, the dependence of the complex dielectric permittivity ε^* on the frequency ω is described by the Havriliak-Negami eq. (24):

$$\varepsilon^*(\omega) = \varepsilon_\infty + \frac{\varepsilon_0 - \varepsilon_\infty}{[1 + (i\omega\tau)^\alpha]^\beta}, \quad (24)$$

where ε_∞ and ε_0 are the dielectric permittivity at extremely high and low frequencies, τ is the relaxation time, α and β are the parameters generalizing various types of relaxation: $\alpha = \beta = 1$ (Debye equation), $\alpha = 0$ and $\beta \neq 0$ (Cole-Davidson equation), $\alpha \neq 0$ and $\beta = 0$ (Cole-Cole equation).

In the presence of Ag NPs, low-temperature peaks on the curves $\varepsilon''(\omega)$ correspond to a shift of β-relaxation to high frequencies, which most likely characterizes the plasticization effect. The same argument can be used to explain the decrease in the activation energy from 61 (matrix) to 50 kJ/mol (4.1 wt.% Ag) in the Arrhenius dependence $\tau(T)$.

The temperature dependence $\log\sigma_{dc} = \phi(1/T)$ of the direct current conductivity of films characterized by different content of Ag myristate is shown in Fig. 22. For reference, the range of glass transition temperatures $T_g = 383$–388 K obtained by DSC is shown by a black rectangle in Fig. 22. It can be seen that two regions are observed in the dependence: the regions above and below T_g. Curves show different behavior in these regions. Thus, in the case of the high-temperature region, the dependence of the Vogel-Fulcher-Tammann type is observed. Experiments [135, 136] show that the values of eq. (20), parameters T_0 and B, do not depend on the concentration of Ag NPs within the error within the studied concentration range. These facts show that joint motion has a significant effect on the change in viscosity of the system with decreasing temperature. The Arrhenius temperature dependence, characterized by an activation energy of about 1.2 eV, is observed at temperatures below T_g.

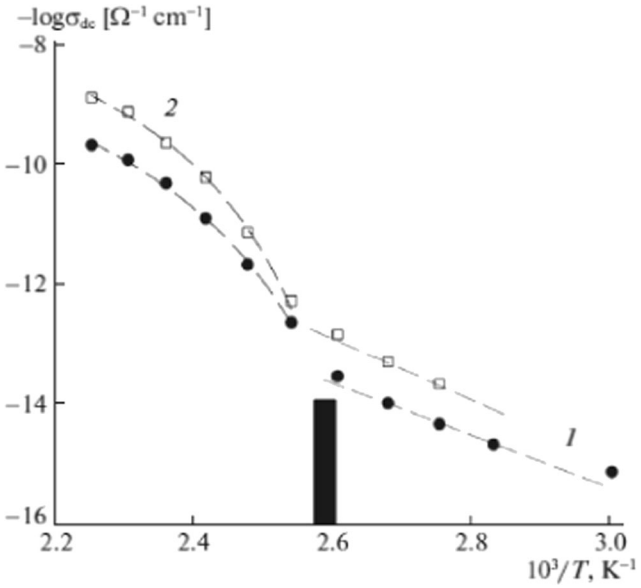

Fig. 22 Temperature dependences of the dc-conductivity of nanocomposite films based on ED20 epoxy oligomer with different concentrations of Ag myristate: (*1*) 0.032, (*2*) 0.7 wt.%; the black rectangle shows the range of T_g obtained via DSC. The data are taken from [135]

The observed shape of the temperature dependence [135] is associated with a change in the mechanism of conductivity after the "freezing" of ionic mobility in this temperature region. Low-temperature peaks on $\varepsilon''(\omega)$, corresponding to β relaxation, are shifted toward high frequencies in the presence of Ag NPs, which probably characterizes the effect of plasticization. The decrease in activation energy from 61 kJ/mol (0.63 eV) (matrix) to 50 kJ/mol (0.52 eV) (4.1 wt.% Ag) in the case of the Arrhenius $\tau(T)$ dependence is associated with the same effect. Thus, the activation energy of β relaxation was about 2 times lower than that determined in these experiments based on the direct current conductivity in the same temperature range at low concentrations of NPs. Despite the differences between the ΔE values, these data to a certain extent correspond to each other. In fact, the direct current conductivity involves long-distance transfer of charges and the breakthrough of barriers, and the β-relaxation process is localized in small areas. This fact requires a detailed study of the processes of electric dipole relaxation. It should be noted that the data obtained correspond to the results of studies [137] of the frequency dependences of the complex electric modulus M^*. The peaks on the curves of complex component M'' of the electric modulus associated with interfacial polarization also shift toward the high-frequency region as the Ag concentration is increases, and the activation energy values calculated on basis of the temperature dependence of their frequency increase to 159 kJ/mol (1.6 eV), which indicates an increase in the heterogeneity of the system.

The peaks on the curves of the imaginary part M'' of the electric modulus M^* (12), which relate to interfacial

polarization, are also shifted to high frequencies with increasing concentration of Ag and activation energies calculated by temperature dependence of their frequency increase to 159 kJ/mol, most demonstrating an increase in system heterogeneity.

Magnetic properties

It is obvious that the magnetic properties of epoxy nanocomposites are determined by NPs, which have a magnetic moment. In particular, magnetite Fe_3O_4 is characterized by a high saturation magnetization (M_c ~ 92–100 emu/g at room temperature). Therefore, when incorporated into the polymer matrix, magnetite can be widely used in applications such as magnetic resonance imaging, biomedical sensors, electromagnetic interference shielding, flexible electronics, magneto-optical storage devices, etc. However, since surface functional groups capable of reacting with an epoxy matrix are in short supply, Fe_3O_4 NPs easily participate in agglomeration due to the strong magnetic dipole-dipole interaction between the particles.

In [138], magnetic epoxy nanocomposites were obtained. The functionalization of Fe_3O_4 NPs by polyaniline was carried out using surface-initiated polymerization.

Experiments have shown that in epoxy nanocomposites containing 15 wt.% both functionalized and non-functionalized NPs at room temperature, there was no magnetic hysteresis loop. Its absence on all magnetization curves with almost zero coercivity indicates the superparamagnetic behavior of composites. This is apparently due to the fact that the size of magnetite NPs is below the critical value (10–20 nm), so that each particle can serve as single magnetic domain with a high constant magnetic moment and can behave like a huge paramagnetic atom. This NP can quickly respond to an applied magnetic field with low coercivity and negligible residual magnetization.

For all samples, the saturation magnetization M_c was not achieved even when a strong magnetic field H was applied. This parameter was estimated by extrapolating dependence $M_c(H^{-1})$. The calculated values of M_c for NPs were much lower than for bulk Fe_3O_4 samples: the level of magnetization for 15% epoxy nanocomposite was about 9.5 emu/g.

Jacobsite $MnFe_2O_4$, whose NPs were used to produce magnetic epoxy nanocomposites [139], exhibits a ferromagnetic behavior, being a magnetite. Table 7 shows the magnetic characteristics of the composite compared with crystalline $MnFe_2O_4$: the coercivity H_c, the saturation magnetization M_c and the magnetic moment m. The growth of coercivity and magnetic moments for nanocomposites can be associated with the presence of hydrogen bonds in the epoxy matrix. The composite magnetization is determined by the dimension of the network of hydrogen bonds with their coordinated motion, which plays the role of exchanging paths between magnetic centers and causing their remagnetization [140]. The value of M_c is influenced by the dipole interaction of NPs, which grows with the concentration of the filler. It seems that this discovery may provide an explanation for the data given in Table 7.

Table 7 Magnetic properties of epoxy nanocomposites with $MnFe_2O_4$ [139]

System	H_c (Oe)	M_c (emu/g)	m (μ_B)
Neat $MnFe_2O_4$	14.9	31.68	1.244
5% nanocomposite	44.7	1.84	1.373
10% nanocomposite	43.9	4.21	1.354

This dependence is confirmed by data on the magnetic properties of epoxy nanocomposites containing inclusions of barium ferrite $BaFe_{12}O_{19}$ NPs (Fig. 23) [141]. It is clear that not only the saturation magnetization (straight line *1*), but also the residual magnetization (straight line *2*) linearly increase with the concentration of $BaFe_{12}O_{19}$. The limiting values of these parameters are 14.0 and 4.1 emu/g, respectively. Note that the coercivity is the same for all systems: H_c = 1.3 kOe.

To impart magnetic properties to epoxy nanocomposites, X. Zhang et al. [142] used graphene with a precipitated product of thermal decomposition of $Fe(CO)_5$ - a mixture of Fe and Fe_2O_3. The saturation magnetization of the composite was 0.04, 0.16, and 0.45 emu/g for 1.0, 3.0, and 5.0 wt.%, respectively. For a neat filler, M_c was 14.7 emu/g. Therefore, the calculated values of M_c for the same concentrations should be 0.15, 0.44, and 0.74 emu/g. According to the authors, the decrease in M_c for NPs can be due to iron oxidation during the curing process.

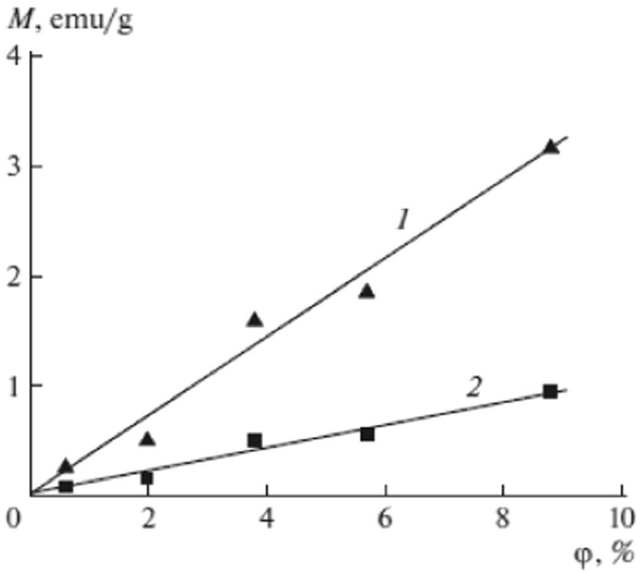

Fig. 23 Dependence of (*1*) saturation magnetization and (*2*) residual magnetization on the volume fraction of the $BaFe_{12}O_{19}$ filler. The data are taken from [141]

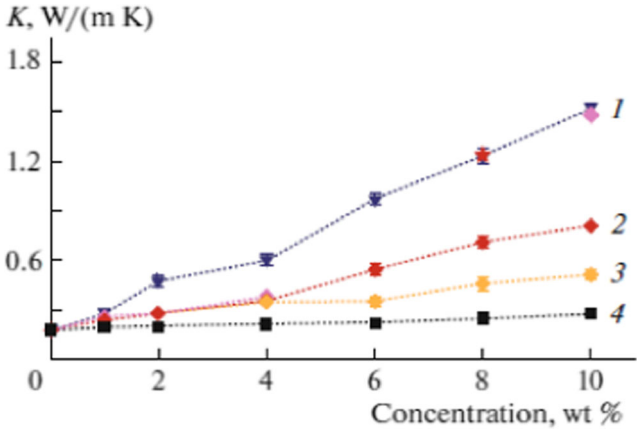

Fig. 24 The concentration dependence of thermal conductivity K of epoxy nanocomposites with fillers: (*1*) graphene, (*2*) MWCNTs, (*3*) GO, and (*4*) graphite. The data are taken from [146]

The coercivity is inversely proportional to the filler content: 67.2, 46.5, and 12.3 Oe, respectively.

In order to protect iron (and other variable valence metals) from further oxidation, NPs with a core-shell structure are used, and noble metals, carbon, and iron oxides are used as a shell [143]. The last metal was used in [144]: Fe (core) + FeO (shell) with a particle size of 15–25 nm and an oxide thickness of 0.5 nm.

As in the previous cases, the saturation magnetization increases with the concentration of NPs. $M_c = 17$ emu/g for epoxy nanocomposites with 20 wt.% NPs. This value is ~16% of the corresponding value of the block filler. With dispersion, the coercivity increases from 62.33 to 202.13 Oe. This observation can be explained by the weakening of the interparticle dipole interaction due to the increase in the distance between single-domain NPs compared with NPs that are in close contact in the block.

A change of the NP shell from FeO to carbon [145] leads to a decrease in the saturation magnetization and causes an increase in the coercivity. This tendency can also be explained by the deterioration of the interparticle dipole interaction.

Thermal conductivity of epoxy nanocomposites

Thermal conductivity is closely related to electrical conductivity. For example, in metals, according to the Wiedemann-Franz law, the thermal conductivity coefficient K is directly proportional to the electrical conductivity. However, carbon fillers with extremely high thermal conductivity and low specific gravity do not demonstrate the expected improvement in thermal conductivity in epoxy nanocomposites, largely due to their poor dispersion and problems associated with the nature of the interfacial layers, in particular, with the Kapitza thermal resistance R_k.

Figure 24 shows the concentration dependences of the thermal conductivity coefficient K for epoxy nanocomposites with a number of carbon nanofillers [146]. The best results were obtained for graphene flakes (curve *1*), i.e., growth 10 times at 10 wt.% MWCNTs. At the same concentration (curve *2*), the thermal conductivity of the matrix increases about five times. But in this case, the electrical conductivity increases by five to seven orders of magnitude. However, the proportionality between these values (K and σ_{dc}) is preserved if the percolation threshold of MWCNTs is overcome [147]. The same relationship is observed between K and σ_{ac} at lower concentrations of graphene, which was obtained by ultrasound exfoliation of graphite oxide [148].

The important role of the interfacial layer was demonstrated by C.-C. Teng et al. [149], who used poly(glycidylmethacrylate) with a terminal pyrene group for non-covalent functionalization of graphene. The thermal conductivity of epoxy nanocomposites containing ~4 wt.% of these NPs was 1.91 W/(m K), which is ~20% higher than in the case of non-functionalized graphene. The thermal resistance of the boundary layer, which is known as Kapitza thermal resistance, is $R_k \approx 8 \times 10^{-8}$ m^2/(K W). This value applies not only to CNTs and other carbon fillers in epoxy matrices, but also to other composite materials and polycrystals [150]. Even a small increase in R_k entails a noticeable deterioration in the thermal conductivity of composite, despite the high values of the thermal conductivity coefficient and the aspect ratio of NPs. As revealed by molecular dynamics modeling using SiC NPs, taking into account the contributions of Kapitza resistance and effective interfacial layer to the overall thermal conductivity is a common and important analytical consideration when analyzing the thermal properties of epoxy nanocomposites, in particular, the effect of particle size [151].

In accordance with [152], for NPs with a small aspect ratio with a volume fraction $\phi \geq \phi_c$ percolation theory gives (25):

$$\ln\left(\frac{\lambda}{\lambda_f}\right) = \left(\frac{1-\phi}{1-\phi_c}\right)^n \times \ln\left(\frac{\lambda_c}{\lambda_f}\right) \quad (25)$$

Here λ, λ_f, and λ_c are thermal conductivity of the composite, filler and percolation concentration ϕ_c. The index n depends on the size and shape of the filler and the character of its distribution in the composite.

Since a noticeable increase in the thermal conductivity of polymer composites is possible only above the percolation threshold, the use of metal NPs for this purpose presents a problem. Indeed, for particles with an

aspect ratio of the order of unity $\phi_c \sim 0.15$; that is, the weight fraction of metallic filler is extremely high. An example is paper [153], in which K is 27 W/(m K) with a volume content of silver NPs of 45%, which corresponds to a weight concentration of 86%.

Tribological properties

Polymer composite coatings have many advantages, for example, resistance to oxidation, to acids and alkalis, possess chemical stability and anti-friction ability. The advantage of polymer nanocomposites as materials for friction units is their increased strength characteristics associated with the interaction features of polymer-nanoparticle: NPs are firmly held in the matrix, and their separation does not change the surface properties. Epoxy polymers occupy an important place among the materials used as coatings [154]. An increase in the strength characteristics of polymeric materials usually leads to a decrease in the coefficient of friction (COF) and wear in friction pairs. These goals are achieved through the use of carbon nanofillers, such as CNT, graphene, fullerene [155].

The self-lubricating property of carbon fiber in polymer composites has been found to improve wear resistance by reducing COF [156]. CNT additives improve the tribological properties of the composite, i.e., the combination of carbon fibers and CNT has a strong synergistic effect [157, 158]. Indeed, as follows from the data [157], shown in Table 8, COF of a composite containing short carbon fibers (μ_0) decreases after adding 0.1 wt.% CNT ($\mu_{0.1}$).

Graphene is a promising material due to the fact that it can form on the contact surface a self-lubricating film with a low and stable COF and wear, which is deposited from a polymer nanocomposite in the process of friction [159, 160]. With increasing graphene content (up to 4%) COF and wear rate of the composite coating are gradually reduced [159]. GO is more effective than graphene [160].

Liu et al. conducted a comparative study of the tribological properties of epoxy coatings with fullerene C_{60} and graphene as fillers [161]. For better dispersion and compatibility with the matrix, both fillers were functionalized with 3-aminopropyltriethoxysine. COF of coatings based on epoxy nanocomposites initially decreased and gradually increased after the content of C_{60} and graphene was higher than 0.5 wt.%. But it was even lower than for epoxy resin. A significant decrease in COF for nanocomposite coatings may be due to self-lubricating fillers as a result of the formation of a continuous film between the steel surface and the rough composite coating. The addition of C_{60} showed better tribological and scratch resistance properties compared to graphene. Those results indicate that the properties of epoxy nanocomposite coatings can strongly depend on the shape of the filler.

Table 8 COF (μ) of epoxy composite coatings on concentration of carbon fibers

Fiber (wt.%)	0	0	5	10	15	20
$\mu_{0.1}/\mu_0$	0.58	0.48	0.38/0.50	0.34/0.45	0.40/0.51	0.42/0.51

R.K. Upadhyay and A. Kumar conducted [162] a comparative study of fullerene C_{70} and CNT as additives (1, 3, 5%) to epoxy coatings, which improve tribological properties. They showed that COF of C_{70} and MWCNT substrates was in the range of 0.17–0.29, 0.07–0.27, respectively, the wear rate was in the range of 10^{-3}–10^{-2} mm^3/N·m. The minimum value of the indicators refers to 3% of the first additive and 1% of the second.

The use of hybrid NPs has proven to be a very effective way to control the tribological properties of coatings based on epoxy nanocomposites. For example, the inclusion of MWCNT-GO hybrid with a low content in the epoxy matrix led to a significant increase in tribological performance [163]. As shown in Fig. 25, in the absence of CNTs, the use of GO leads to an increase in COF, although the wear rate is significantly reduced. However, in the presence of CNT, COF decreases the more, the higher the concentration of GO. The wear rate also decreases at low concentrations of GO, although as it grows, wear also increases.

According to the authors of [163], these phenomena are due to the following reasons. First, the dispersion of CNTs in the epoxy matrix was significantly improved using 0.1 phr GO. Secondly, the introduction of GO can increase the adhesion/interlocking of the nanofiller-epoxy resin and the glass transition temperature [164].

Conclusions

An analysis of the data examined suggests that significant experimental material on epoxy nanocomposite materials reinforced with carbon nanotubes has been accumulated by now, indicating the intensity of the development of their chemistry. To date, the basic principles of designing such nanocomposites have been formulated, their structural organization is understood, and development trends in this area are relatively well

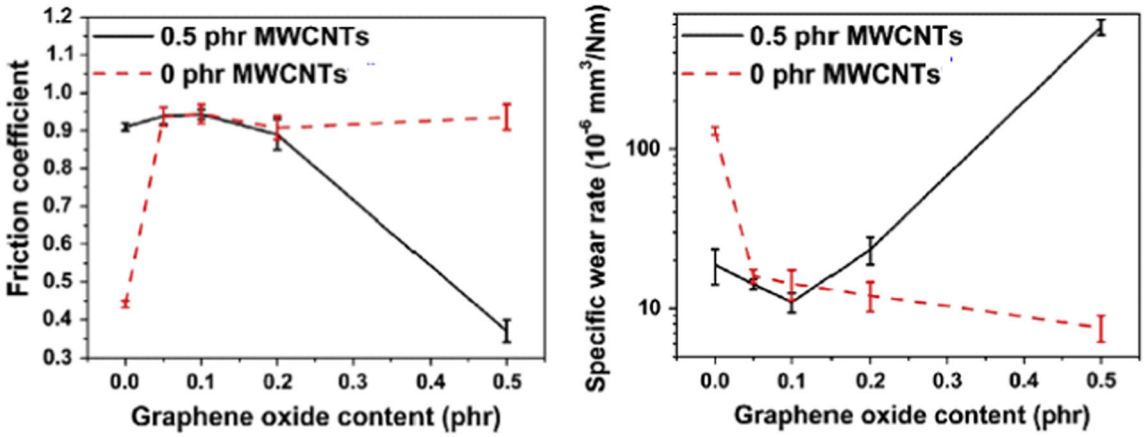

Fig. 25 The friction coefficient and the specific wear rate for the GO/epoxy composites [152] and hybrid MWCNT-GO/epoxy composites with 0.5 phr MWCNTs and different GO contents tested under 1 MPa and 1 m/s. The data are taken from [163]

represented. It should be emphasized that the molecular design of epoxy nanocomposites is an important, and in some cases, a defining problem for both the targeted production of such materials with predetermined properties and their subsequent use. Due to their improved mechanical, electrophysical, magnetic, thermal and tribological properties, epoxy nanocomposites can be widely used in the aerospace field, as laminates and sandwich structures, anti-lightning, anti-radar protection devices, flame retardant and heat-resistant paints, ameliorating anti-corrosion performances, etc.

How do we present the prospects for the development of this interesting area of nanocomposite materials?

First, it is a search for greater "accuracy" in the directional synthesis of epoxy nanocomposites with controlled composition, size and functionality, which allow targeted development of nanocomposite materials with desired properties. As already noted, the properties of polymer nanocomposites are determined by the structure of the matrix, the type and nature of the distribution of nanofillers in the bulk, and finally, the size and nature of the interfacial layer. This is especially true for epoxy nanocomposites, including a wide range of carbon nanofillers. At this level, the greatest attention should be paid to a clearer definition of the specificity of epoxy matrices, their chain nature and transformations that they undergo in the process of obtaining nanocomposites. Among the most important tasks in this direction is the further development and optimization of methods for producing epoxy nanocomposites reinforced with carbon nanotubes for target applications. Of particular interest is the study of the influence of the conditions for obtaining epoxy nanocomposites on their final properties and composition. Without any doubt, such research directions will become a guideline for investigation of epoxy nanocomposites in the near future.

It can be concluded that, although in some aspects of chemistry of epoxy nanocomposites reinforced with carbon nanotubes there is still no complete clarity, the intensity of research in this area ensures that the successful solution of many problems is unquestionable.

Abbreviations *BADGE*, Diglycidyl ether of bisphenol A; *CNT*, Carbon nanotube; *COF*, Coefficient of friction; *3DG*, Three-dimensional graphene product; *GO*, Graphene oxide; *MMT*, *Montmorillonite*; *MWCNT*, Multiwall carbon nanotube; *NP*, Nanoparticle; *SEM*, Scanning electron microscopy; *SWCNT*, Single-walled carbon nanotube

References

1. Reshetnyak OV, Zaikov GE (eds) (2017) Computational and experimental analysis of functional materials. Apple Academic Press, CRC Press, Waretown
2. Pascault J-P, Williams RJJ (eds) (2010) Epoxy polymers: new materials and innovations. Wiley, Weinheim
3. Jin F-L, Li X, Park S-J (2015) Synthesis and application of epoxy resins: a review. J Ind Eng Chem 29:1–11
4. Chen S, Xu Z, Zhang D (2018) Synthesis and application of epoxy-ended hyperbranched polymers. Chem Eng J 343:283–302
5. Irzhak VI, Rozenberg BA, Enikolopyan NS (1979) Cross-linked polymers. Synthesis, structure, properties, Nauka, Moscow [in Russian]
6. Rozenberg BA (1986) Kinetics, thermodynamics and mechanism of reactions of epoxy oligomers with amines. Adv Polym Sci 75: 113–165
7. Okabe T, Takehara T, Inose K, Hirano N, Nishikawa M, Uehara T (2013) Curing reaction of epoxy resin composed of mixed base resin and curing agent: experiments and molecular simulation. Polymer 54:4660–4668
8. Huang M, Shen Z, Wang Y, Li H, Luo T, Lei Y (2019) Thermomechanical properties and morphology of epoxy resins with copoly (phthalazinone ether nitrile). J Polym Res 26:96
9. Zhou C, Li R, Luo W, Chen Y, Zou H, Liang M, Li Y (2016) The preparation and properties study of polydimethylsiloxane-based coatings modified by epoxy resin. J Polym Res 23:14
10. Lin J, Wu X, Zheng C, Zhang P, Li Q, Wang W, Yang Z (2014) A novolac epoxy resin modified polyurethane acylates polymer

grafted network with enhanced thermal and mechanical properties. J Polym Res 21:435
11. Mittal V (ed) (2016) Spherical and fibrous filler composites. Wiley, Weinheim
12. Motavalli M, Czaderski C, Schumacher A, Gsell D (2010) In: Pohl G (ed) Textiles, polymers and composites for buildings. Elsevier, Amsterdam, pp 69–128
13. Ebrahimi F (ed) (2012) Nanocomposites - new trends and developments. InTech, Rijeka
14. Gu H, Ma C, Gu J, Guo J, Yan X, Huang J, Zhang Q, Guo Z (2016) An overview of multifunctional epoxy nanocomposites. J Mater Chem C 4:5890–5906
15. Irzhak TF, Irzhak VI (2017) Epoxy nanocomposites. Polym Sci, Ser A 59:791–825
16. Mittal V (2014) Polymer nanotubes nanocomposites: synthesis, properties and applications. Wiley, Weinheim
17. Kablov EN, Kondrashov SV, Yurkov GY (2013) Prospects of using carbonaceous nanoparticles in binders for polymer composites. Nanotechnol Russ 8:163–185
18. Sahoo NG, Rana S, Cho JW, Li L, Chan SH (2010) Polymer nanocomposites based on functionalized carbon nanotubes. Prog Polym Sci 35:837–867
19. Irzhak VI (2011) Epoxide composite materials with carbon nanotubes. Russ Chem Rev 80:787–806
20. Ates M, Eker AA, Eker B (2017) Carbon nanotube-based nanocomposites and their applications. J Adhes Sci Technol 31:1977–1997
21. Roy S, Petrova R, Mitra S (2018) Effect of carbon nanotube (CNT) functionalization in epoxy-CNT composites. Nanotechnol Rev 7:475–485
22. Song YS, Youn JR (2005) Influence of dispersion states of carbon nanotubes on physical properties of epoxy nanocomposites. Carbon 43:1378–1385
23. Valentini L, Armentano I, Puglia D, Kenny JM (2004) Dynamics of amine functionalized nanotubes/epoxy composites by dielectric relaxation spectroscopy. Carbon 42:323–329
24. Tamburri E, Orlanducci S, Terranova ML, Valentini F, Palleschi G, Curulli A, Brunetti F, Passeri D, Alippi A, Rossi M (2005) Modulation of electrical properties in single-walled carbon nanotube/conducting polymer composites. Carbon 43:1213–1221
25. Sun L, Warren GL, O'Reilly JY, Everett WN, Lee SM, Davis D, Lagoudas D, Sue HJ (2008) Mechanical properties of surface-functionalized SWCNT/epoxy composites. Carbon 46:320–328
26. Sun L, Warren GL, Davis D, Sue H-J (2011) Nylon toughened epoxy/SWCNT composites. J Mater Sci 46:207–214
27. Farhadinia M, Arab B, Jam JE (2016) Mechanical properties of CNT-reinforced polymer Nano-composites: a molecular dynamics study. Mech Adv Compos Struct 3:113–121
28. Song SH, Park KH, Kim BH, Choi YW, Jun GH, Lee DJ, Kong BS, Paik KW, Jeon S (2013) Enhanced thermal conductivity of epoxy–graphene composites by using non-oxidized graphene flakes with non-covalent functionalization. Adv Mater 25:732–737
29. Du J, Cheng H-M (2012) The fabrication, properties, and uses of graphene/polymer composites. Macromol Chem Phys 213:1060–1077
30. Monetta T, Acquesta A, Bellucci F (2015) Graphene/epoxy coating as multifunctional material for aircraft structures. Aerospace 2:423–434
31. Atlukhanova LB, Kozlov GV (2018) A carbon nanotubes aggregation in polymer nanocomposites. Mater Sci Forum 935:55–60
32. Ren F, Zhu G, Wang Y, Cui X (2014) Microwave absorbing properties of graphene nanosheets/epoxy-cyanate ester resins composites. J Polym Res 21:585
33. Wu Q, Li M, Gu Y, Li Y, Zhang Z (2014) Nano-analysis on the structure and chemical composition of the interphase region in carbon fiber composite. Compos Part A Appl Sci Manuf 56:143–149
34. Diez-Pascual AM, Gómez-Fatou MA, Ania F et al (2015) Nanoindentation in polymer nanocomposites. Prog Mater Sci 67:1–94
35. Zhao Y-L, Stoddart JF (2009) Noncovalent functionalization of single-walled carbon nanotubes. Acc Chem Res 42:1161–1171
36. Terrones M, Martin O, González M et al (2011) Interphases in graphene polymer-based nanocomposites: Achievements and challenges. Adv Mater 23:5302–5310
37. Britz DA, Khlobystov AN (2006) Noncovalent interactions of molecules with single walled carbon nanotubes. Chem Soc Rev 35:637–659
38. Summ BD, Ivanova NI (2000) The use of objects and methods of colloid chemistry in nanochemistry. Russ Chem Rev 69:911–923
39. Kozlov GV (2015) Structure and properties of particulate-filled polymer nanocomposites. Physics-Uspekhi 58:33–60
40. Georgakilas V, Otyepka M, Bourlinos AB, Chandra V, Kim N, Kemp KC, Hobza P, Zboril R, Kim KS (2012) Functionalization of graphene: covalent and non-covalent approaches, derivatives and applications. Chem Rev 112:6156–6214
41. Kong L, Enders A, Rahman TS, Dowben PA (2014) Molecular adsorption on graphene. J Phys Condens Matter 26:443001–443028
42. Yuan P, Tan D, Annabi-Bergaya F (2015) Properties and applications of halloysite nanotubes: recent research advances and future prospects. Appl Clay Sci 112-113:75–93
43. Lvov Y, Abdullayev E (2013) Green and functional polymer - clay nanotube composites with sustained release of chemical agents. Prog Polym Sci 38:1690–1791
44. Jagtap SB, Rao VS, Barman S, Ratna D (2015) Nanocomposites based on epoxy resin and organoclay functionalized with a reactive modifier having structural similarity with the curing agent. Polymer 63:41–71
45. Aufray M, Roche AA (2008) Is gold always chemically passive? Study and comparison of the epoxy-amine/metals interphases. Appl Surf Sci 254:1936–1941
46. Mercier D, Rouchaud JC, Barthès-Labrousse MG (2008) Interaction of amines with native aluminum oxide layers in non-aqueous environment: application to the understanding of the formation of epoxy-amine/metal interphases. Appl Surf Sci 254:6495–6503
47. Henz BJ, Hawa T, Zachariah MR (2008) Mechano-chemical stability of gold nanoparticles coated with alkanethiolate SAMs. Langmuir 24:773–783
48. Jiménez A, Sarsa A, Blázquez M et al (2010) A molecular dynamics study of the surfactant surface density of alkanethiol self-assembled monolayers on gold nanoparticles as a function of the radius. J Phys Chem 114:21309–21314
49. Hostetler MJ, Wingate JE, Zhong C-J, Harris JE, Vachet RW, Clark MR, Londono JD, Green SJ, Stokes JJ, Wignall GD, Glish GL, Porter MD, Evans ND, Murray RW (1998) Alkanethiolate gold cluster molecules with core diameters from 1.5 to 5.2 nm: Core and monolayer properties as a function of core size. Langmuir 14:17–30
50. Badamshina ER, Gafurova MP, Estrin YI (2010) Modification of carbon nanotubes and synthesis of polymeric composites involving the nanotubes. Russ Chem Rev 79:945–979
51. Seong M, Kim DS (2015) Effects of facile amine-functionalization on the physical properties of epoxy/graphene nanoplatelets nanocomposites. J Appl Polym Sci 132:42269–42275
52. Sun P, Liu G, Lv D et al (2016) Simultaneous improvement in strength, toughness, and thermal stability of epoxy/halloysite nanotubes composites by interfacial modification. J Appl Polym Sci 133:43249–43257

53. Sahoo NG, Cheng HKF, Li L, Chan SH, Judeh Z, Zhao J (2009) Specific Functionalization of Carbon Nanotubes for Advanced Polymer Nanocomposites. Adv Funct Mater 19:3962–3971
54. Rubio N, Au H, Leese HS, Hu S, Clancy AJ, Shaffer MSP (2017) Grafting from versus grafting to approaches for the functionalization of graphene nanoplatelets with poly(methyl methacrylate). Macromolecules 50:7070–7079
55. Zdyrko B, Luzinov I (2011) Polymer brushes by the "grafting to" method. Macromol Rapid Commun 32:859–869
56. Allaoui A, El Bounia N-E (2009) How carbon nanotubes affect the cure kinetics and glass transition temperature of their epoxy composites? – a review. Express Polym Lett 3:588–594
57. Putz KW, Palmeri MJ, Cohn RB, Andrews R, Brinson LC (2008) Effect of cross-link density on interphase creation in polymer nanocomposites. Macromolecules 41:6752–6756
58. Auad ML, Mosiewicki MA, Uzunpinar C, Williams RJJ (2010) Functionalization of carbon nanotubes and carbon nanofibers used in epoxy/amine matrices that avoid partitioning of the monomers at the fiber interface. Polym Eng Sci 50:183–190
59. Wang S, Liang R, Wang B, Zhang C (2009) Covalent addition of diethyltoluenediamines onto carbon nanotubes for composite application. Polym Compos 30:1050–1057
60. Barber AH, Cohen SR, Kenig S, Wagner HD (2004) Interfacial fracture energy measurements for multi-walled carbon nanotubes pulled from a polymer matrix. Compos Sci Technol 64:2283–2289
61. Zhang Y, Wang Y, Yu J, et. al. (2014) Tuning the interface of graphene platelets/epoxy composites by the covalent grafting of polybenzimidazole. Polymer 55: 4990–5000
62. Wan Y-J, Gong L-X, Tang L-C, Wu LB, Jiang JX (2014) Mechanical properties of epoxy composites filled with silane-functionalized graphene oxide. Compos Part A Appl Sci Manuf 64:79–108
63. Wan Y-J, Tang L-C, Gong L-X, Yan D, Li YB, Wu LB, Jiang JX, Lai GQ (2014) Grafting of epoxy chains onto graphene oxide for epoxy composites with improved mechanical and thermal properties. Carbon 69:467–480
64. Deng H, Wu F, Chen L et al (2014) Enhanced interfacial interaction of epoxy nanocomposites with activated graphene nanosheets. J Appl Polym Sci 131:41164–41171
65. Li Z, Wang R, Young RJ, Deng L, Yang F, Hao L, Jiao W, Liu W (2013) Control of the functionality of graphene oxide for its application in epoxy nanocomposites. Polymer 54:6437–6446
66. Shanmugharaj AM, Yoon JH, Yang WJ, Ryu SH (2013) Synthesis, characterization, and surface wettability properties of amine functionalized graphene oxide films with varying amine chain lengths. J Colloid Interface Sci 401:148–154
67. Guan L-Z, Wan Y-J, Gong L-X, Yan D, Tang LC, Wu LB, Jiang JX, Lai GQ (2014) Toward effective and tunable interphases in graphene oxide/epoxy composites by grafting different chain lengths of polyetheramine onto graphene oxide. J Mater Chem A 2:15058–15069
68. Konnola R, Joji J, Parameswaranpillai J, Joseph K (2015) Structure and thermo-mechanical properties of CTBN-grafted-GO modified epoxy/DDS composites. RSC Adv 5:61775–61801
69. Becker O, Simon GP (2005) Epoxy layered silicate nanocomposites. Adv Polym Sci 179:29–82
70. Paiva LB, de Morales AR, Valenzuela Diaz FR (2008) Organoclays: properties, preparation and applications. Appl Clay Sci 42:8–24
71. Yang L, Phua SL, Teo JKH, Toh CL, Lau SK, Ma J, Lu X (2011) A biomimetic approach to enhancing interfacial interactions: Polydopamine-coated clay as reinforcement for epoxy resin. ACS Appl Mater Interfaces 3:3026–3032
72. Jlassi K, Chandran S, Poothanari MA, Benna-Zayani M, Thomas S, Chehimi MM (2016) Clay/polyaniline hybrid through diazonium chemistry: conductive nanofiller with unusual effects on interfacial properties of epoxy nanocomposites. Langmuir 32: 3514–3545
73. Du M, Guo B, Jia J (2010) Newly emerging applications of halloysite nanotubes: a review. Polym Int 59:574–582
74. Prashantha K, Lacrampe M-F, Krawczak P (2013) Halloysite nanotubes-polymer nanocomposites: a new class of multifaceted materials. Adv Mater Manufact Charact 3:11–14
75. Gooding JJ, Ciampi S (2011) The molecular level modification of surfaces: from self-assembled monolayers to complex molecular assemblies. Chem Soc Rev 40:2704–2718
76. Ghorai PK, Glotzer SC (2007) Molecular dynamics simulation study of self-assembled monolayers of alkanethiol surfactants on spherical gold nanoparticles. J Phys Chem C 111:15857–15862
77. Kaushik AP, Clancy P (2012) Explicit all-atom modeling of realistically sized ligand-capped nanocrystals. J Chem Phys 136: 114702–114714
78. Christensen RM (1979) Mechanics of composite materials. Wiley, New York
79. Zhuang GS, Sui GX, Sun ZS, Yang R (2006) Pseudoreinforcement effect of multiwalled carbon nanotubes in epoxy matrix composites. J Appl Polym Sci 102:3664–3672
80. Ayatollahi M, Shadlou S, Shokrieh M et al (2011) Effect of multi-walled carbon nanotube aspect ratio on mechanical and electrical properties of epoxy-based nanocomposites. Polym Test 30:548–556
81. Omidi M, Rokni HDT, Milani AS et al (2010) Prediction of the mechanical characteristics of multi-walled carbon nanotube/epoxy composites using a new form of the rule of mixtures. Carbon 48: 3218–3228
82. Martone A, Faiella G, Antonucci V, Giordano M, Zarrelli M (2011) The effect of the aspect ratio of carbon nanotubes on their effective reinforcement modulus in an epoxy matrix. Compos Sci Technol 71:1117–1123
83. Hsieh TH, Kinloch AJ, Taylor AC, Kinloch IA (2011) The effect of carbon nanotubes on the fracture toughness and fatigue performance of a thermosetting epoxy polymer. J Mater Sci 46:7525–7535
84. Choi WJ, Powell RL, Kim DS (2009) Curing behavior and properties of epoxy nanocomposites with amine functionalized multi-wall carbon nanotubes. Polym Compos 30:415–421
85. Chen X, Wang J, Lin M, Zhong W, Feng T, Chen X, Chen J, Xue F (2008) Mechanical and thermal properties of epoxy nanocomposites reinforced with amino-functionalized multi-walled carbon nanotubes. Mater Sci Eng A 492:236–242
86. Yoonessi M, Lebrón-Colón M, Scheiman D, Meador MA (2014) Carbon nanotube epoxy nanocomposites: the effects of interfacial modifications on the dynamic mechanical properties of the nanocomposites. ACS Appl Mater Interfaces 6:16621–16630
87. Ma PC, Mo SY, Tang BZ, Kim JK (2010) Dispersion, interfacial interaction and re-agglomeration of functionalized carbon nanotubes in epoxy composites. Carbon 48:1824–1834
88. Lachman N, Wagner HD (2010) Correlation between interfacial molecular structure and mechanics in CNT/epoxy nano-composites. Compos Part A Appl Sci Manuf 41:1093–1098
89. Grachev VP, Kondrashov SV, Akatenkov RV et al (2014) Modification of epoxy polymers by small additives of multiwall carbon nanotube. Polym Sci, Ser A 56:330–336
90. Corcione C, Freuli F (2013) The aspect ratio of epoxy matrix nanocomposites reinforced with graphene stacks. Polym Eng Sci 53:531–539
91. Wang X, Jin J, Song M (2013) An investigation of the mechanism of graphene toughening epoxy. Carbon 65:324–333
92. Rafiee MA, Rafiee J, Wang Z, Song H, Yu ZZ, Koratkar N (2009) Enhanced mechanical properties of nanocomposites at low graphene content. ASC Nano 3:3884–3890

93. Martin-Gallego M, Bernal MM, Hernandez M, Verdejo R, Lopez-Manchado MA (2013) Comparison of filler percolation and mechanical properties in graphene and carbon nanotubes filled epoxy nanocomposites. Eur Polym J 49:1347–1353
94. Sun X, Sun H, Li H, Peng H (2013) Developing polymer composite materials: carbon nanotubes or graphene? Adv Mater 25: 5153–5176
95. Tang X, Zhou Y, Peng M (2015) Green preparation of epoxy/graphene oxide nanocomposites using a glycidylamine epoxy resin as the surface modifier and phase transfer agent of graphene oxide. ACS Appl Mater Interfaces 8:1854–1894
96. Park JK, Kim DS (2014) Effects of an aminosilane and a tetrafunctional epoxy on the physical properties of di-functional epoxy/graphene nanoplatelets nanocomposites. Polym Eng Sci 54:969–976
97. Wang F, Drzal LT, Qin Y et al (2016) Effects of functionalized graphene nanoplatelets on the morphology and properties of epoxy resins. High Perform Polym 28:525–536
98. Krishnamoorthy K, Veerapandian M, Yun K, Kim SJ (2013) The chemical and structural analysis of graphene oxide with different degrees of oxidation. Carbon 53:38–49
99. Ni Y, Chen L, Teng K, Shi J, Qian X, Xu Z, Tian X, Hu C, Ma M (2015) Superior mechanical properties of epoxy composites reinforced by 3D interconnected graphene skeleton. ACS Appl Mater Interfaces 7:11583–11591
100. Kusmono K, Wildan MW, Mohd Ishak ZA (2013) Preparation and properties of clay-reinforced epoxy nanocomposites. Int J Polym Sci 2013:ID690675–ID690682
101. Wang M, Fan X, Thitsartarn W, He C (2015) Rheological and mechanical properties of epoxy/clay nanocomposites with enhanced tensile and fracture toughnesses. Polymer 58:43–52
102. Jia QM, Zheng M, Xu CZ, Chen HX (2006) The mechanical properties and tribological behavior of epoxy resin composites modified by different shape nanofillers. Polym Adv Technol 17: 168–173
103. Rafiee M, Yavari F, Rafiee J et al (2011) Fullerene-epoxy nanocomposites – enhanced mechanical properties at low nanofiller loading. J Nanopart Res 13:733–737
104. Zuev VV (2012) The mechanisms and mechanics of the toughening of epoxy polymers modified with fullerene C_{60}. Polym Eng Sci 52:2518–2522
105. Pikhurov DV, Zuev VV (2014) The effect of fullerene C_{60} on the mechanical and dielectrical behavior of epoxy resins at low loading. AIP Conf Proc 1599:453–456
106. Javidparvar AA, Ramezanzadeh B, Ghasemi E (2016) Effects of surface morphology and treatment of iron oxide nanoparticles on the mechanical properties of an epoxy coating. Prog Org Coat 90: 10–21
107. Sun T, Fan H, Wang Z, Liu X, Wu Z (2015) Modified nano Fe_2O_3-epoxy composite with enhanced mechanical properties. Mater Des 87:10–32
108. Al-Ajaj IA, Abd MM, Jaffer HI (2013) Mechanical properties of micro and nano TiO_2/epoxy composites. International journal of mining. Metallurgy & Mechanical Engineering (IJMMME) 1:93–97
109. Bogdanova LM, Kuzub LI, Dzhavadyan EA, Torbov VI, Dremova NN, Pomogailo AD (2014) Mechanical properties of epoxy composites based on silver nanoparticles formed in situ. J Polym Sci, Ser A 56:304–310
110. Stauffer G, Author (1985) Introduction to percolation theory. Taylor and Francis, London
111. Li J, Ma PC, Chow WS, To CK, Tang BZ, Kim JK (2007) Correlations between percolation threshold, dispersion state, and aspect ratio of carbon nanotubes. Adv Funct Mater 17:3207–3215
112. Guadagno L, De Vivo B, Di Bartolomeo A et al (2011) Effect of functionalization on the thermo-mechanical and electrical behavior of multi-wall carbon nanotube/epoxy composites. Carbon 49:1919–1930
113. Liu L, Etika KC, Liao K-S, Hess LA, Bergbreiter DE, Grunlan JC (2009) Comparison of covalently and noncovalently functionalized carbon nanotubes in epoxy. Macromol Rapid Commun 30: 627–632
114. Rakov EG (2013) Carbon nanotubes in new materials. Russ Chem Rev 82:27–47
115. Ivanovskii AL (2012) Graphene-based and graphene-like materials. Russ Chem Rev 81:571–605
116. An J-E, Jeong YG (2013) Structure and electric heating performance of graphene/epoxy composite films. Eur Polym J 49:1322–1330
117. Vavouliotis A, Fiamegou E, Karapappas P, Psarras GC, Kostopoulos V (2010) Dc and ac conductivity in epoxy resin/multiwall carbon nanotubes percolative system. Polym Compos 31:1874–1880
118. Seidel GD, Lagoudas DC (2009) A micromechanics model for the electrical conductivity of nanotube-polymer nanocomposites. J Compos Mater 43:917–942
119. Thakre PR, Bisrat Y, Lagoudas DC (2010) Electrical and mechanical properties of carbon nanotube-epoxy nanocomposites. J Appl Polym Sci 116:191–202
120. Yuen SM, Ma CM, Wu HH et al (2007) Preparation and thermal, electrical, and morphological properties of multiwalled carbon nanotube and epoxy composites. J Appl Polym Sci 103:1272–1278
121. Tsonos B, Kanapitsas A, Psarras GC et al (2015) Effect of ZnO nanoparticles on the dielectric/electrical and thermal properties of epoxy-based nanocomposites. Sci Adv Mater 7:588–597
122. Martinez-Garcia JC, Rzoska SJ, Drozd-Rzoska A, Starzonek S, Mauro JC (2015) Fragility and basic process energies in vitrifying systems. Sci Rep 5:8314–8320
123. Mathioudakis GN, Patsidis AC, Psarras GC (2014) Dynamic electrical thermal analysis on zinc oxide/epoxy resin nanodielectrics. J Therm Anal Calorim 116:27–33
124. Patsidis A, Psarras GC (2008) Dielectric behaviour and functionality of polymer matrix – ceramic $BaTiO_3$ composites. Express Polym Lett 2:718–726
125. Singha S, Thomas MJ (2008) Dielectric properties of epoxy nanocomposites. IEEE Trans Dielectr Electr Insul 15:12–23
126. Singha S, Thomas MJ (2009) Influence of filler loading on dielectric properties of epoxy-ZnO nanocomposites. IEEE Trans Dielectr Electr Insul 16:531–542
127. Wang Q, Chen G (2014) Effect of pre-treatment of nanofillers on the dielectric properties of epoxy nanocomposites. IEEE Trans Dielectr Electr Insul 21:1809–1816
128. Huang X, Xie L, Yang K, Wu C, Jiang P, Li S, Wu S, Tatsumi K, Tanaka T (2014) Role of interface in highly filled epoxy/$BaTiO_3$ nanocomposites. Part I-correlation between nanoparticle surface chemistry and nanocomposite dielectric property. IEEE Trans Dielectr Electr Insul 21:467–479
129. Gonon P, Boudefel A (2006) Electrical properties of epoxy/silver nanocomposites. J Appl Phys 99:024308–024316
130. Chiteme C, McLachlan DS (2003) Ac and dc conductivity, magnetoresistance, and scaling in cellular percolation systems. Phys Rev B 67:024206–024223
131. Nam S, Cho HW, Kim T et al (2011) Effects of silica particles on the electrical percolation threshold and thermomechanical properties of epoxy/silver nanocomposites. Appl Phys Lett 99:043104–043107
132. Cho HW, Nam S, Lim S et al (2014) Effects of size and interparticle interaction of silica nanoparticles on dispersion and electrical conductivity of silver/epoxy nanocomposites. J Appl Phys 115: 154307–154314

133. Vescovo L, Sangermano M, Scarazzin R et al (2010) In-situ-synthetized silver/epoxy nanocomposites: electrical characterization by means of dielectric spectroscopy. Macromol Chem Phys 211:1933–1939
134. Kortaberria G, Sangermano M, Mondragon I (2012) In situ synthetized silver/epoxy nanocomposites: electrical characterization in terms of dielectric relaxation spectroscopy. Macromol Symp 321-322:112–117
135. Novikov GF, Rabenok EV, Bogdanova LM et al (2017) Dielectric properties of films of ag-ED20 epoxy nanocomposite synthesized in situ. Temperature dependence of direct current conductivity. Polym Sci Ser A 59:741–750
136. Novikov GF, Rabenok EV, Bogdanova LM et al (2017) Temperature dependence of direct current conductivity in ag-ED20 nanocomposite films. Russ J Phys Chem A 91:1971–1975
137. Kortaberria G, Arruti P, Modragon I et al (2011) Dynamics of in situ synthetized silver-epoxy nanocomposites as studied by dielectric relaxation spectroscopy. J Appl Polym Sci 120:2361–2367
138. Gu H, Tadakamalla S, Huang Y, Colorado HA, Luo Z, Haldolaarachchige N, Young DP, Wei S, Guo Z (2012) Polyaniline stabilized magnetite nanoparticle reinforced epoxy nanocomposites. ACS Appl Mater Interfaces 4:5613–5624
139. Huang J, Cao Y, Zhang X, Li Y, Guo J, Wei S, Peng X, Shen TD, Guo Z (2015) Magnetic epoxy nanocomposites with superparamagnetic $MnFe_2O_4$ nanoparticles. AIP Adv 5:097183–097198
140. KR O'N, Brinzari TV, Wright JB et al (2014) Pressure-induced magnetic crossover driven by hydrogen bonding in $CuF_2(H_2O)_2$(3-chloropyridine). Sci Rep 4:6054–6059
141. Kanapitsas A, Tsonos C, Psarras GC, Kripotou S (2016) Barium ferrite/epoxy resin nanocomposite system: fabrication, dielectric, magnetic and hydration studies. Express Polym Lett 10:227–237
142. Zhang X, Alloul O, He Q, Zhu J, Verde MJ, Li Y, Wei S, Guo Z (2013) Strengthened magnetic epoxy nanocomposites with protruding nanoparticles on the graphene nanosheets. Polymer 54: 3594–3604
143. Wei S, Wang Q, Zhu J, Sun L, Lin H, Guo Z (2011) Multifunctional composite core–shell nanoparticles. Nanoscale 3:4474–4502
144. Zhu J, Wei S, Ryu J, Sun L, Luo Z, Guo Z (2010) Magnetic epoxy resin nanocomposites reinforced with core-shell structured Fe@FeO nanoparticles: fabrication and property analysis. ACS Appl Mater Interfaces 2:2100–2107
145. Zhang X, Alloul O, Zhu J, He Q, Luo Z, Colorado HA, Haldolaarachchige N, Young DP, Shen TD, Wei S, Guo Z (2013) Iron-core carbon-shell nanoparticles reinforced electrically conductive magnetic epoxy resin nanocomposites with reduced flammability. RSC Adv 3:9453–9464
146. Song SH, Park KH, Kim BH, Choi YW, Jun GH, Lee DJ, Kong BS, Paik KW, Jeon S (2013) Enhanced thermal conductivity of epoxygraphene composites by using non-oxidized graphene flakes with non-covalent functionalization. Adv Mater 25:732–743
147. Bonnet P, Sireude D, Garnier B, Chauvet O (2007) Thermal properties and percolation in carbon nanotube-polymer composites. Appl Phys Lett 91:201910–201913
148. Corcione C, Freuli F, Maffezzoli A (2012) The aspect ratio of epoxy matrix nanocomposites reinforced with graphene stacks. Polym Eng Sci 53:531–539
149. Teng C-C, C-CM M, Lu C-H et al (2011) Thermal conductivity and structure of non-covalent functionalized graphene/epoxy composites. Carbon 49:5107–5116
150. Nan C-W, Liu G, Lin Y, Li M (2004) Interface effect on thermal conductivity of carbon nanotube composites. Appl Phys Lett 85: 3549–3551
151. Yu S, Yang S, Cho M (2011) Multiscale modeling of cross-linked epoxy nanocomposites to characterize the effect of particle size on thermal conductivity. J Appl Phys 110:124302–124311
152. Zhang G, Xia Y, Wang H et al (2010) A percolation model of thermal conductivity for filled polymer composites. J Compos Mater 44:963–971
153. Pashayi K, Fard HR, Lai F, Iruvanti S, Plawsky J, Borca-Tasciuc T (2012) High thermal conductivity epoxy-silver composites based on selfconstructed nanostructured metallic networks. J Appl Phys 111:104310–104316
154. Liu D, Zhao W, Liu S, Cen Q, Xue Q (2017) In situ regulating of surface morphologies, anti-corrosion and tribological properties of epoxy resin coatings by heat treatment. Surf Topogr 5:024003–024013
155. Zhai W, Srikanth N, Kong LB, Zhou K (2017) Carbon nanomaterials in tribology. Carbon 119:150–171
156. Dhieb H, Buijnsters J, Eddoumy F et al (2011) Surface damage of unidirectional carbon fiber reinforced epoxy composites under reciprocating sliding in ambient air. Compos Sci Technol 71: 1769–1776
157. Gbadeyan OJ, Kanny K, Turup Pandurangan M (2018) Tribological, mechanical, and microstructural of multiwalled carbon nanotubes/short carbon fiber epoxy composites. J Tribol 140: 022002–022029
158. Shivamurthy B, Murthy K, Anandhan S (2018) Tribology and mechanical properties of carbon fabric/MWCNT/epoxy composites. Adv Tribol 2018 article ID 1508145/1-10
159. Zhang Y, Zhang D, Wei X, Zhong S, Wang J (2018) Enhanced tribological properties of polymer composite coating containing graphene at room and elevated temperatures. Coatings 8:91–102
160. Wu F, Zhao W, Chen H et al (2016) Interfacial structure and tribological behaviours of epoxy resin coating reinforced with graphene and graphene oxide. Surf Interface Anal 49:85–92
161. Liu D, Zhao W, Liu S, Cen Q, Xue Q (2016) Comparative tribological and corrosion resistance properties of epoxy composite coatings reinforced with functionalized fullerene C_{60} and graphene. Surf Coat Technol 286:354–364
162. Upadhyay RK, Kumar A (2018) A novel approach to minimize dry sliding friction and wear behavior of epoxy by infusing fullerene C_{70} and multiwalled carbon nanotubes. Tribol Int 120:455–464
163. Shen X-J, Pei X-Q, Liu Y, Fu SY (2014) Tribological performance of carbon nanotube–graphene oxide hybrid/epoxy composites. Compos B Eng 57:120–125
164. Shen X-J, Pei X-Q, Fu S-Y, Friedrich K (2013) Significantly modified tribological performance of epoxy nanocomposites at very low graphene oxide content. Polymer 54:1234–1242